Environmental Science Nano

ROYAL SOCIETY OF CHEMISTRY

TUTORIAL REVIEW

View Article Online
View Journal | View Issue



Check for updates

Cite this: *Environ. Sci.: Nano*, 2021, **8**, 3452

# Bioengineering applications of black phosphorus and their toxicity assessment

Na Wu, †[ab] Xiaomei Wang, †[a] Chandreyee Manas Das, [c] Mingze Ma, [b] Nan Qiao, [b] Taojian Fan, [d] Han Zhang, *[d] Gaixia Xu *[b] and Ken-Tye Yong *[cef]

Received 23rd March 2021,
Accepted 21st September 2021

DOI: 10.1039/d1en00273b

rsc.li/es-nano

During the last decade, 2-dimensional nanoscale black phosphorus (NBP) has been actively used for biomedical research and applications. NBP possesses unique properties such as an adjustable direct band gap, high near-infrared (NIR) photothermal conversion efficiency, large surface area for versatile surface chemistry functionalization and good biodegradability for *in vivo* delivery and therapy. Many groups have reported that functionalized NBP can be applied for biomedical applications. However, untreated NBP is unstable and if it is applied biologically, it might trigger harmful nano-bio interactions and cause adverse effects on the biological system permanently. In this review, we summarized the bioengineering applications of NBP, including biosensing, photoimaging, photo-X therapy and drug delivery. Then, the various nano–bio interactions that occurred during the use of NBP for bioengineering research with an emphasis on examining the adverse impacts of NBP on the integrity of the cell membrane structure were analyzed. The *in vivo* instability of NBP inducing phagocytosis, increasing the levels of many kinds of cytokines in the blood, and resulting in various responses to the body was discussed systematically. Based on our analysis, the *in vitro* and *in vivo* toxicity of NBP can be reduced by strategically functionalizing its surface with biocompatible materials such as hydrogels, polymers and fibrin.

### Environmental significance

Recently, nanoscale black phosphorus (NBP) has been actively used for biomedical research and applications. Some research studies have suggested that NBP is more suitable to be applied for biological therapies since its by-products from degradation may be removed from the body easily. However, what effect will NBP cause in the environment and organisms is unclear yet. It is important for us to examine and investigate the biocompatibility of NBP *in vitro* and *in vivo*. In this review, we first discuss the preparation and functionalization of NBP, then talk about the bioengineering applications of NBP followed by the types of toxicity assessment of NBP *in vitro* and *in vivo*, which will give a future outlook of NBP materials in the bioengineering field.

## 1 Introduction

The successful discovery of the single-layer graphite material was reported by Novoselov *et al.*[1] in 2004, which created an opportunity for scientists to fabricate various 2-dimensional (2D) nanomaterials. Among them, 2D transition metal disulfides (TMDs) display semiconducting property which was not found in common graphene. Due to their unique physical and chemical properties, such novel nanomaterials have prompted various research groups to study and apply them for applications ranging from electronics to biomedical imaging.[2,3] In the following decade, many of the emerging 2D nanomaterials such as monoelemental germanene,[4] xene,[5] stanine[6] and so on were synthesized and used in bioengineering.[7–10] In 2014, Li *et al.* reported for the first time layered nanoscale black phosphorus (NBP) from a silica substrate.[11] The direct band gap of 2D NBP can be adjusted by tailoring its composition and it has been used for improving the performance of photodetectors[12,13] and photoelectric sensors.[14]

Phosphorus (P), an element that can be easily oxidized and decomposed into phosphate, is abundant in biological organisms. It is an important component in biofilm and

[a] *Department of Physiology, International Carson Center, School of Health Science Center, Shenzhen University, Shenzhen, 518055, China*
[b] *Guangdong Key Laboratory for Biomedical Measurements and Ultrasound Imaging, School of Biomedical Engineering, Health Science Center, Shenzhen University, Shenzhen, 518055, China. E-mail: xugaixia@szu.edu.cn*
[c] *School of Biomedical Engineering, The University of Sydney, Sydney, NSW 2006, Australia. E-mail: ken.yong@sydney.edu.au*
[d] *Collaborative Innovation Center for Optoelectronic Science and Technology of Shenzhen University, Shenzhen, 518060, China. E-mail: hzhang@szu.edu.cn*
[e] *The University of Sydney Nano Institute, The University of Sydney, Sydney, NSW 2006, Australia*
[f] *The Biophotonics and MechanoBioengineering Lab, The University of Sydney, Sydney, NSW 2006, Australia*
† First authors.

nucleic acids, and also aids in the energy metabolism of cells.[15] Therefore, some studies have suggested that 2D NBP was more suitable to be applied for biological applications since its by-products after degradation were nontoxic and may be removed from the body easily.[16] However, further studies are needed to confirm this speculation. To date, many groups have applied functionalized NBP for bioengineering research such as tumor-targeted photothermal therapy, photothermal–chemo combination therapy,[17,18] photothermal gene combination therapy,[19] photodynamic therapy, and photoacoustic imaging.[20,21]

With the ever-increasing bioengineering publications on the NBP material, there is a rising concern about the safety of NBP for *in vivo* studies. We have no idea about the nano–bio interface between NBP and animals, the toxicity after NBP degradation *in vivo*, and the safe dosage of NBP for imaging or therapy. What's more, nobody knows whether there are other harmful byproducts created and how to clear them from the body. All of these questions have not been answered so far. Most of the publications have generally focused on its applications. Thus, it is important for us to examine and investigate the biocompatibility of NBP *in vitro* and *in vivo*. Previous studies have clearly indicated that nanomaterials will eventually lead to *in vitro* and *in vivo* toxicity.[22,23] Various factors of nanomaterials, such as composition, crystal structure, synthesis method, size and thickness, surface functionalization and solubility, determine their toxicity impacts.[24,25] Recently, some studies have shown that untreated black phosphorus-based quantum dots (BPQDs) and black phosphorus nanosheets (BPNSs) displayed mild toxicity effects on HeLa cells at concentrations of 1000 ppm and 100 ppm, respectively.[26,27] However, other studies reported otherwise. For instance, Mu *et al.* observed cytotoxicity on HeLa cells when the cells were treated with 200 ppm of BPQDs.[28] Based on the reported literature, it is challenging for researchers to determine the toxicity of NBP and the relationship between such toxicity and the nano–bio interactions at the cellular level. Thus, in this review, we discussed the preparation of functionalized NBP for bioengineering applications, and summarized the NBP *in vitro* and *in vitro* toxicity from the view of the nano–bio interactions (Scheme 1). Finally, we proposed the future outlook of NBP materials in the bioengineering field in a broad term.

## 2 Preparation and functionalization of NBP

### 2.1 Preparation and challenges in healthcare applications of NBP

**2.1.1 Preparation and surface functionalization of NBP.** The biocompatibility of nanomaterials generally depends on their synthesis methods and surface modification procedures. In this section, we review and analyze the various preparation methods of NBP and the various types of surface modification techniques used for bioengineering research.

In general, bulk black phosphorus (BP) is stable at high temperature and pressure but this changes when it is made at the nanoscale level. For example, the reaction activity between P and the surrounding oxygen was discovered to increase significantly due to its large surface area that caused NBP to become unstable.[29] Layers of NBP were first obtained from the bulk sample by using a scotch tape[11] and the produced NBP had high purity and fewer defects. However, it was difficult to control the size, shape and thickness of NBP using this approach. In 2014, Brent *et al.* invented a liquid exfoliation technique to prepare NBP.[30] They placed bulk BP into 1-methyl-2-pyrrolidone (NMP) solvent and thereafter the system was exposed to high-power ultrasound waves (820 W, 37 kHz) for 24 h. The supernatant was separated to obtain NBP with a lateral size of 200 nm and a thickness between 3.5 and 5 nm. Later, Lin *et al.* compared the exfoliation effect in the presence of different organic solvents such as ethanol, acetone, NMP and isopropanol by using the same liquid

**Na Wu**

*Na Wu received her B.S. degree in Photoelectric Engineering in 2014 from Shenzhen University. From 2014–2017, she got her master's degree in Biophotonics from Shenzhen University. Her research interests include biomedical imaging and nano toxicology of nanoparticles including semi-conducting quantum dots, polymer dots, and 2-dimensional nanomaterials.*

**Xiaomei Wang**

*Xiaomei Wang received her Ph.D. in Biology from Jilin University in 2002. From 2002 to 2004, she completed her postdoctoral fellowship in Basic Medical School, Shantou University. She has been in Shenzhen University since 2004 and got her full professor appointment in 2006. Her research interests include the toxicity of various nanomaterials and cancer gene therapy. In recent years, she has published more than 100 research papers in these fields, including Aging-US, Nanomedicine: Nanotechnology, Biology, and Medicine, Chem. Soc. Rev.*

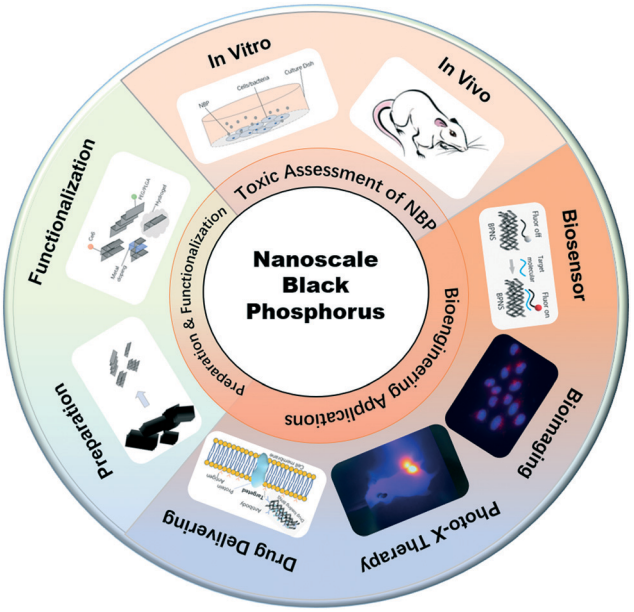


Scheme 1 An overall structure of this review.

exfoliation procedure mentioned above (Fig. 1A) and the group found that the highest yield could be achieved with isopropanol solvent.[31] Also, further separation by centrifugation of the sample allowed one to obtain different batches of NBP with smaller sizes and shapes.[32] It was reported that NBP-based QDs with a diameter of 2.6 ± 1.8 nm and a thickness of 1.5 ± 0.6 nm could be synthesized effectively by employing a probe and water bath ultrasound together with BP powder.[33] Zhu *et al.* reported a liquid shear stripping method to produce 2–3 nm BPQDs and these particles were referred to as phosphorene.[34] Similarly, Sofer *et al.* prepared 80–200 nm NBP particles by mixing BP powder with an organic solvent and treating the mixture with ultrasound waves followed by grinding the black phosphorus suspension in different organic solvents (NMP, DMF DIGLYM and AN) with an ultra Turrax disperser (Fig. 1B).[35]

The solvothermal method is an alternative way to synthesize BPQDs.[36,37] Upon mixing BP powder with the NMP solvent, the mixture was stirred vigorously at 140 °C for 6 hours where BPQDs were generated with an average size of 2.1 ± 0.9 nm (Fig. 1C).[38] Since the BP atomic layers are attached together *via* van der Waals force, 70 nm sized BP nanoparticles could be prepared by the electrochemical exfoliation method (Fig. 1D). This method is suitable to make larger sizes of NBP particles.[39] Pulsed laser ablation (PLA) is another good tool to make NBP. Firstly, bulk BP is placed at the bottom of a cuvette and protected with nitrogen saturated isopropanol (IPE) solution. A Nd:YAG pulsed laser (10 Hz) with a wavelength of 1064 nm was then focused on the BP crystals and the BP crystals were irradiated for 30 minutes until a pale yellow supernatant appeared (Fig. 1E). XPS and Raman spectra revealed that the resulting supernatant was composed of 5–14 nm BPQDs with a thickness of about 1.1 nm.[40] The quantum yield of BPQDs is estimated to be 20.7%, which is two times higher than that of BPQDs prepared by the liquid exfoliation method,[26] and it is worth commenting that the quantum yield of BPQDs can be maintained at 12% after 12 days of preparation.[41]

**2.1.2 Challenges of using NBP in healthcare applications.** To prevent NBP from oxidizing and degrading, it has to be kept in an organic solvent. According to Huang *et al.*, BP flakes were not able to dissolve in $O_2$ de-aerated water and insignificant degradation was observed in the BP layered structure. However, when BP was placed in $O_2^-$ rich de-ionized water for 2 days, the majority of BP flakes degraded. When BP flakes were exposed to air for one day, a large fraction of O elements (Fig. 2A) appeared on their surface, the ratio of $P_0 : P_xO_y$ in water was 2.3, which was found to be much higher than that in air (0.24), and this indicates that BP is highly prone to getting oxidized by $O_2$, but not by water dissociation. The untreated BP surface is hydrophobic but it can become hydrophilic upon oxidation.[42] Thus, it is inevitable for NBP to lose its optical and semiconductor properties if its surface is not properly shielded from $O_2$. Photo-oxidation is another cause of degradation,[43] without proper surface modification, NBP can generate oxygen free radicals under visible light irradiation and this can create toxic effects in the biological system.[44] When untreated NBP is mixed with *ex vivo* whole blood, plasma proteins are attached to the surface of NBP which creates a BP–corona complex. Such phenomena will not only change the hydrodynamic diameter of BPQDs and NBPs but also induce adverse inflammatory response in the human body.[45] Therefore, there remain substantial challenges to be overcome before one can safely use NBP for various clinical bioengineering applications such as *in vivo* targeted imaging. To overcome these challenges, few approaches were developed. For example, Poudel *et al.* demonstrated the preparation of an NBP drug loaded nanocarrier from bulk BP by using a one step process for targeted drug delivery therapy. However, there are some drawbacks from using this approach.[46] For instance, it is challenging to control the size and yield of NBP during the preparation process. Another issue is the abundance of P in the body which means that it is not possible for one to use an inductively coupled plasma-mass spectrometry (ICP-MS) system to determine NBP concentration *in vivo* and thus it is difficult to perform a detailed pharmacokinetic study.

### 2.2 Surface functionalization of NBP

**2.2.1 Improving colloidal and optical stability of NBP.** Light is an important factor that accelerates the oxidation of BP.[44] The main mechanism of photoinduced BP degradation involves the generation of $O_2^-$ species from the BP surface through a charge transfer reaction under exposure to light and thereafter reacting with P on the surface of BP to form $P_xO_y$. To prevent the degradation of NBP *in vitro* or *in vivo*, a few methods were devised. The first method involves coating the surface of NBP with biocompatible materials and this

 

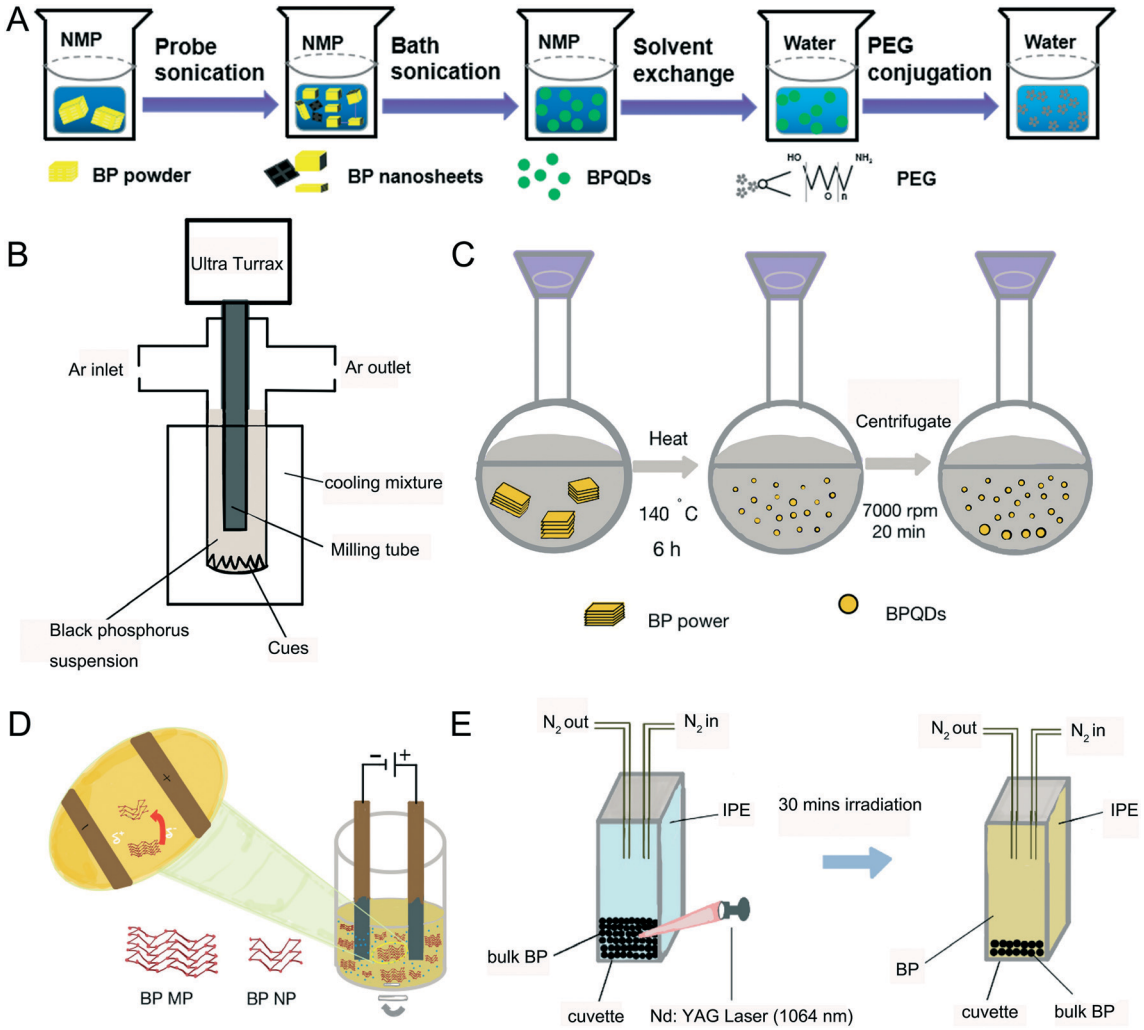


**Fig. 1** Preparation methods of NBP. A) Process of ultrasonic exfoliation. B) Process of the grinding method. C) Process of the solvothermal method. D) Process of electrochemical stripping. E) Process of pulsed laser ablation.

effectively creates a physical barrier between the NBP surface and the atmospheric environment.[33,47] For example, colloidal BPQDs coated with a PLGA polymer material were able to sustain themselves in phosphate-buffered saline (PBS) solution for 8 weeks without the loss of their optical and electronic properties.[48] Surface modifications are useful to block direct contact of P with oxygen and other ions in the biological environment. Tannin (TA) is another useful coating material for preventing BP from being oxidized. It was reported that the lattice fringes and chemical bonds of NBP modified with TA (TA-BP) were intact after being exposed to an ambient environment for 10 days. This is because the superoxidized radicals could be removed by the hydrogen donors from TA. In addition, biocompatible materials such as hydrogels, liposomes and fibrin are often used as surface coating agents for NBP, which allows one to create NBP carriers to achieve reasonably good therapeutic effects of photothermal and photodynamic therapy *in vitro* and *in vivo*.[27,49–51] On the other hand, Walia *et al.* reported the use of an ionic liquid agent to modify the NBP surface which thus created a chemical barrier for the NBP complex. This barrier not only blocked the reactive oxygen species (ROS) generation on the NBP surface but also helped to protect the electronic properties of the material.[52]

**2.2.2 Enhancing the photothermal conversion efficiency.** NBP possesses high photothermal conversion efficiency in the NIR region and this means that it has a deeper tissue penetration depth when compared to that in the visible light band. In general, when light is delivered to the tumor site for photo-therapy application, the light significantly attenuates when it reaches a few cm deep inside the tumor matrix. This is due to the light dispersion effect caused by the thick tumor tissue. Under this constraint, it is not possible to achieve successful tumor ablation using the classical photothermal therapy approach. To overcome this issue, Yang *et al.*[53] prepared an NBP complex named BP@PEG-Ce6 NS and the nanoformulation contained a commercial photosensitizer called chilrin 6 (Ce6). The modification of Ce6 on the NBP effectively enhanced the photothermal conversion efficiency of the NBP complex from 28.7% to 43.6%, which greatly

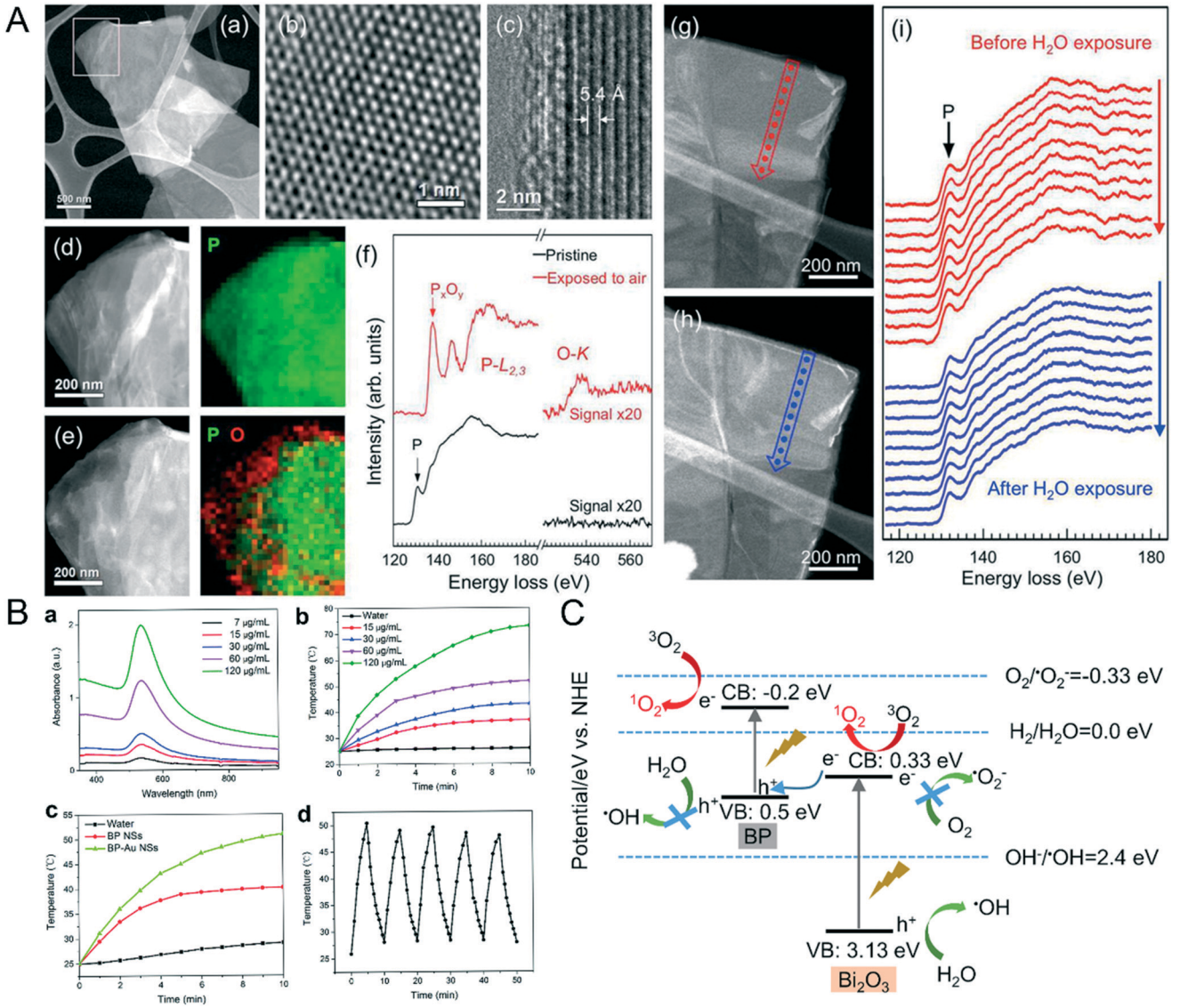


**Fig. 2** A) Oxidization of BP NPs in oxygen surrounding. HAADF STEM image (a) and high-resolution TEM image (b) of a BP flake freshly exfoliated are shown first, (c) is the cross-sectional TEM image of a folded section of flake, (d) showed the enlarge TEM image of the rectangular area in (a) with the corresponding 2D STEM-EELS map, P is shown in green. (e) showed the STEM image and 2D STEM-EELA map of BP flake after 1 day air exposure, P is in green and O is in red, (f) is the EELS spectral of pristine BP and air oxidative BP exposed in water, HAADF-STEM images of freshly BP flake before (g) and after (h) submersion in DI water and the corresponding EELS line scan (i) displayed that no detectable oxidization happened in the L-edge of BP. Reprinted from Huang *et al.*[42] Copyright 2016 American Chemical Society. B) Photothermal conversion efficiency and stability of NBP enhanced by Au modification including the absorbance (a), temperature trends (b) of different BP-Au NS concentrations under 808 nm laser, temperature curve of 60 μg $mL^{-1}$ BP NS and BP-Au NS (c) and temperature variation of BP-Au NS of five laser on/off cycles. Reprinted from Yang *et al.*[54] Copyright The Royal Society of Chemistry 2017. C) Principle of $^1O_2$ generation increased by doping of Bi. Reprinted from Huang *et al.*[57] Copyright 2018 Elsevier Ltd.

improved the efficacy of photothermal therapy. Also, Yang and his coworkers[54] attached gold nanoparticles on the BPNS surface to promote its photothermal therapy efficiency. The temperature of 120 μg $ml^{-1}$ BP-Au NS was increased rapidly from 25 °C to above 70 °C after the formulation was irradiated by an 808 nm laser with a power density of 2 W $cm^{-2}$ for 10 minutes. The photothermal conversion efficiency was estimated to be 43.57% (Fig. 2B) for the BP-Au NS formulation. More recently, Shao *et al.*[55] mixed thermosensitive hydrogel [poly(D,L-lactide)-poly(ethylene glycol)-pol (D,L-lactide) (PDLLA-PEG-PDLLA:PLEL)] with NBP and prepared a formulation (BP@PLEL) that was capable of performing sol–gel switching in the NIR wavelength. BP@PLEL was in a sol state at room temperature but when it was sprayed and deposited onto a living body (~37 °C), it quickly turned into a gel state and then into the sol state after being irradiated with NIR light. This approach allows one to eradicate solid cancer edge tissues in the body. Studies have shown that this material is reasonably compatible with some biological systems but it was also shown that it can effectively kill bacteria. Such materials are expected to be useful for potential application such as postoperative

 

eradication of tumor resection since they have excellent photothermal conversion efficiency.

**2.2.3 Advancing the generation of singlet oxygen.** Generation of harmful singlet oxygen to kill cancer cells is the foundation of the photodynamic therapy (PDT) process. Since BP has abundant surface atomic active sites and low electron–hole radiation rates, it is straightforward for NBP to be activated and produce singlet oxygen species under exposure to NIR light irradiation.[42,56] Huang *et al.* synthesized BP/$Bi_2O_3$ NS nano-heterostructures that could produce high concentration levels of ROS under irradiation of X-rays. With the irradiation of X-rays, the electrons in the conduction band (CB) of $Bi_2O_3$ rapidly combined with the holes in the valence band (VB) of BP which then significantly increased the energy transfer between the excited electrons in BP and the surrounding $^3O_2$ (Fig. 2C) thereby creating $^1O_2$ species for killing cancer cells.[57] Based on the authors' finding, under X-ray illumination, A375 cells produced 55.4% and 38.8% of singlet oxygen upon treatment with 10 mg $ml^{-1}$ BP/$Bi_2O_3$ (1 h) and bare NBP, respectively. This clearly indicates that the addition of $Bi_2O_3$ increases the singlet oxygen production from the NBP complex formulation.[57] Furthermore, the attachment of gold nanoparticles on the NBP surface can also enhance the production of singlet oxygen.[58] It is worth highlighting that Liu *et al.* designed an oxygen self-supply NBP system bearing a passivated catalase on the NBP surface that was coupled with fatty acid (FA) for targeted delivery to the tumor site. When the nanoformulation was delivered to the tumor cells, the attached catalase was activated and thereby triggered the generation of $O_2$ from $H_2O_2$ within the cell. The presence of these generated singlet oxygen species under the irradiation of NIR light was confirmed by the rapid death of cancer cells within a short period of time.[59]

# 3 Therapeutic applications of NBP

## 3.1 Biosensing

As a narrow band gap semiconductor with high carrier mobility and photoelectric conversion characteristics,[60] NBP can be used in a variety of biosensors such as fluorescence, electrochemical, field transistor, chemiluminescence, and electrogenerated chemiluminescence biosensors.[61] Zhou *et al.*[14] used BPNSs as a fluorescence quenching material and developed a sensitive and a rapid biosensor detection platform. The platform not only has a good linear response to microRNA with a concentration of 10 nM to 1000 nM, but also can distinguish trinucleotide polymorphism. Peng *et al.*[62] used Au nanoparticles and a few-layered BP to prepare BP-Au nanoparticles with excellent catalytic activity and low activation energy. The catalytic activity of the BP-Au nanoparticles changed from "inactive" to "active" after being treated with antibodies and antigens and thus provided colorimetric detection results for the detection of biomarkers. The results showed that this biosensor could selectively detect carcinoembryonic antigen (CEA) with a high detection (1 pg $mL^{-1}$ to −10 μg $mL^{-1}$) and sensitivity (0.20 pg $mL^{-1}$) range. Besides, Tuteja *et al.*[63] created an electrochemical immunoassay system for haptoglobin determination based on the electrochemical characteristics of NBP, which could be used to quantitatively detect haptoglobin in serum with a dynamic response range of 0.01–10 mg $ml^{-1}$. Meanwhile Liu *et al.*[64] developed an NBP-based electrochemical luminescence (ECL) biosensing system. The system chose luminol as an energy donor and NBP as an energy acceptor, thereby achieving the quenching effect of NBP on luminol. When the detected object was bound to the surface of NBP through electrostatic interaction, the energy transfer from luminol to NBP was cut off, and the ECL signal reappeared. The quantitative detection of the measured object could be achieved by the dynamic changing intensity of the ECL signal with different concentrations of the measured object. They confirmed that the detection platform could sensitively and quickly detect trypsin in serum. Moreover, Zhou *et al.*[65] invented an NBP integrated fiber sensor, which was immobilized with anti-neuron specific enolase (anti-NSE) cancer biomarkers for the detection of biomarkers containing NSE (Fig. 3). Testing results demonstrated that this biosensor was almost 100 times more sensitive than AuNP- and graphene-based fiber sensors, and had a lower detection limit, as low as 1.0 pg $mL^{-1}$. With all this, it seems that biosensors based on NBP have stable, fast and sensitive response characteristics, and they may lead the biosensor industry to a new stage.

## 3.2 Photoimaging

**3.2.1 Live cell imaging.** In actuality, NBP not only has photothermal response characteristics, but also has photoluminescence properties. It is reported that the photoluminescence effect of NBP depends on its thickness and the distance between its atomic layers; the thinner the thickness, the better the luminescence effect.[66] Lee *et al.* used an ultrasonication assisted solution method to prepare BPQDs with an average diameter of about 10 nm and a height of about 8.7 nm; the quantum yield was about 1.9%. The BPQDs could be excited at 358 nm and 488 nm with emissions at 461 nm and 509 nm, respectively. Confocal imaging (Fig. 4A) showed that these BPQDs clearly labeled the contours of live HeLa cells, which implicated their bioimaging ability.[26] Coincidentally, Ren and his co-workers prepared BPQDs with a thickness of about 1.1 nm and a lateral diameter of 5–14 nm, the quantum yield of BPQDs was up to 20.7%, and they could be effectively used for live cell imaging.[40] The same imaging effect was also verified in the study of Shin *et al.*, who made NBP with a hydrodynamic diameter of 164 ± 24 nm. Cell imaging results verified that NBP could be internalized and concentrated in the cytoplasm of C2C12 cells, and they displayed green fluorescence under the excitation of 495 nm laser radiation.[67] From the cases mentioned above, it can be concluded that its photoluminescence characteristics allow NBP to be used as a fluorescent probe in biomedical imaging.

**3.2.2 Photoacoustic and photothermal imaging.** Photoacoustic imaging (PAI) and photothermal imaging (PTI)

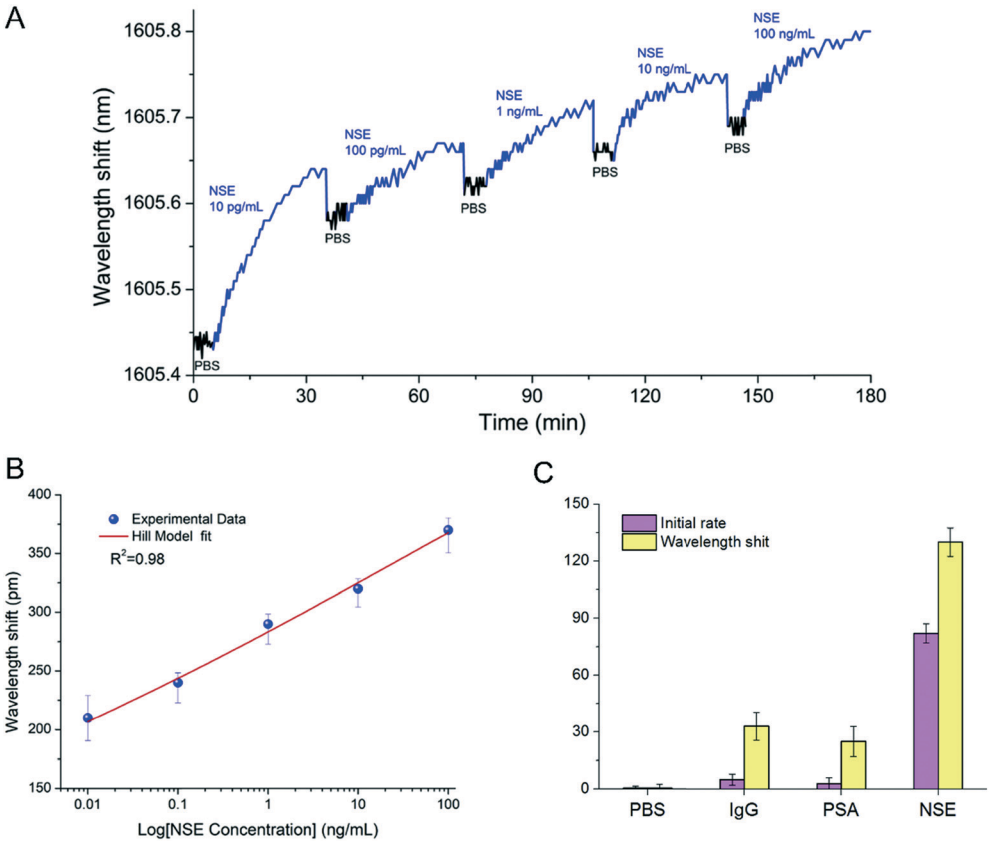


Fig. 3 Label-free detection of NSE with anti-NSE immobilized BP-TFG. (A) Wavelength shift caused by binding interactions with target NSE samples with increasing concentration. (B) Dependence of wavelength shift on NSE concentration. (C) Specificity in PBS, IgG, PSA, and NSE of the BP-TFG biosensor. Reprinted from Zhou *et al.*,[65] Copyright 2019 Elsevier B.V.

are known as non-destructive medical imaging methods. As for PAI, the pulsed laser light radiation is converted into heat energy by a photothermal nanoprobe that causes thermoelastic expansion in tissues; this signal can be picked up by the ultrasound detector for further image reconstruction.[68] In contrast, PTI uses an infrared thermal imager as the thermal signal detector. As a material with excellent photothermal conversion efficiency, NBP can be used to determine the aggregation of tumor sites by photoacoustic imaging after entering *in vivo* surroundings, thus forming a high spatial resolution tumor contour and providing information on spatiotemporal localization for further photothermal and its combination therapy.[69] A previous study reported by Sun *et al.* showed that $TiL_4$-coordinated BPQDs could be used as a contrast agent for photoacoustic imaging, and the addition of $TiL_4$ not only effectively improved the biological stability of BPQDs, but led to the blue absorption peak shift from 808 nm to 680 nm. As shown in Fig. 4B, after entering the mice, the maximum PA signals were observed in 4 hours post injection and they decreased to normal levels the same as that of pre-injection 48 h post-injection, which revealed that the time at 4 hours post-injection was the best time point for treatment; this functional NBP provides us with a better way to monitor the dynamic changes of drug accuracy targeted therapy.[70] As for PTI of NBP, although its spatial resolution is lower than that of PAI, the high signal intensity can also show the distribution of NBP during the process of *in vivo* circulation as well as the dynamic aggregation process in tumor sites, which provides the basis for the best treatment time for photothermal therapy of tumors.[27]

### 3.3 Photo-X therapy

**3.3.1 Photothermal sterilization.** Excessive temperatures (such as above 40 degrees Celsius) are often not suitable for the survival of living organisms, but may be used as a means to inhibit the proliferation of bacteria or viruses. Therefore, scientists use the photothermal effect of NBP for sterilization. Under 808 nm and 0.5 W $cm^{-2}$ laser irradiation, $MoS_2$, graphene and bulk BP did not produce any obvious pro-bactericidal effect on *E. coli* or *S. aureus* bacteria, even after being irradiated for 3 minutes, whereas the sterilization rate of NBP was as high as 99.2%.[71] Additionally, NBP with thinner thickness showed a better antibacterial effect, mainly because the thinner NBP had a larger specific surface area to which bacteria could more likely adhere;[50] thereby it could kill more bacteria under the same irradiation conditions.[72,73] However, since NBP easily degrades in air and aqueous environment, the effect of photothermal sterilization is greatly reduced in a short amount of time.[74] To this end, scientists have tried to modify its surface to improve its

 

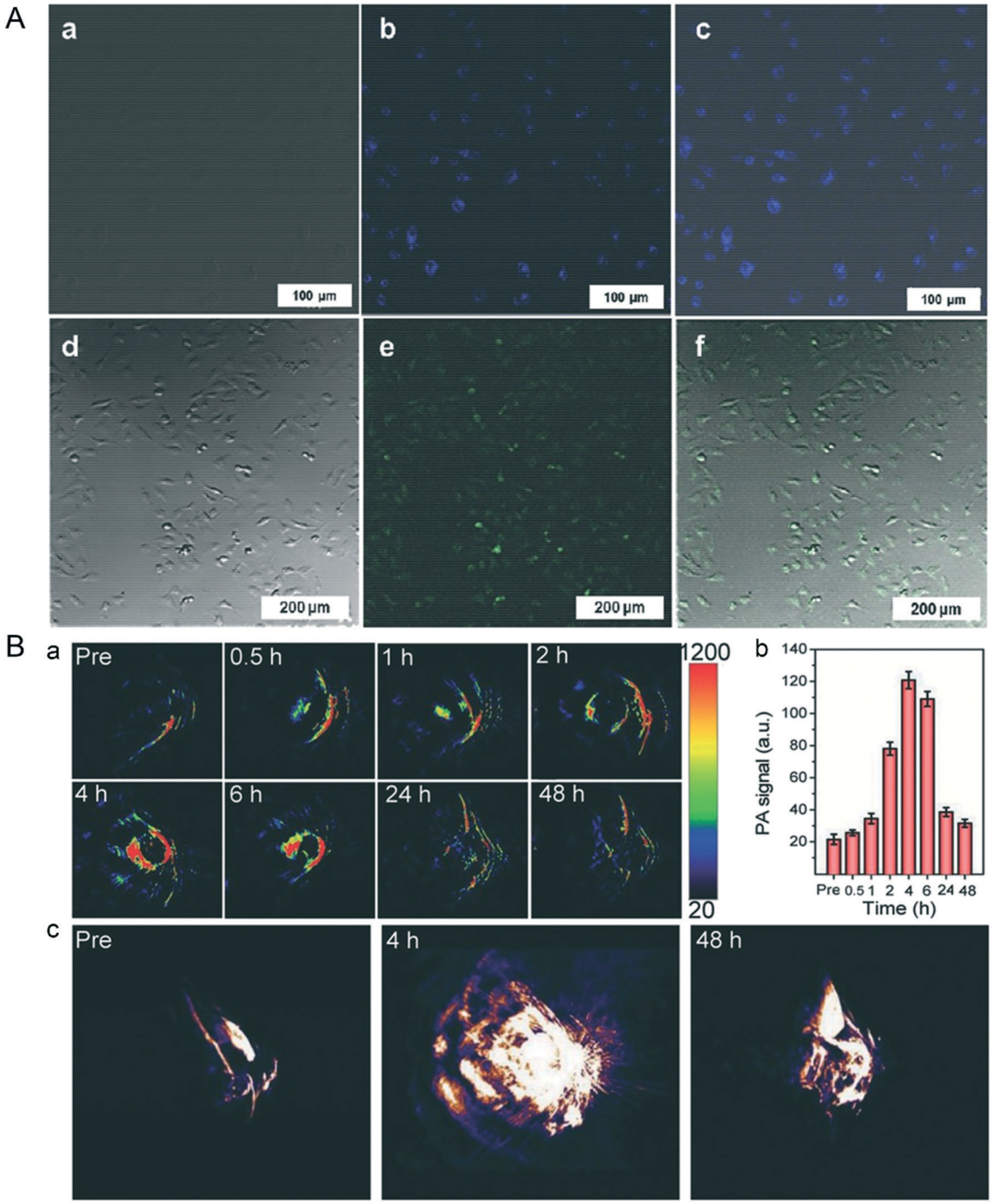


**Fig. 4** A) Confocal microscopy images of live HeLa cells labelled by BPQDs after 12 hours co-incubation, (a and d) bright field and (b and e) fluorescence, and merged (c and f) images. Reprinted from Lee *et al.*[26] Copyright 2015 Wiley-VCH Verlag GmbH & Co. KGaA, Weinheim. B) *In vivo* PA performances of $TiL_4$@BPQDs in MCF-7 tumor-bearing BALB/c nude mice, (a) showed the time-dependent PA image and (b) is the quantitative analysis of each ROI signal in (a), while (c) is the typical 3D PA images of tumor at different time point before and after TiL4@BPQDs injection. Reprinted from Sun *et al.*[70] Copyright 2017 Wiley-VCH Verlag GmbH & Co. KGaA, Weinheim.

stability and photothermal effects. Shao *et al.* found that coating NBP with heat-sensitive PLEL hydrogel (BP@PLEL hydrogel) can not only improve its stability but also effectively improve the overall photothermal conversion efficiency of BP@PLEL hydrogel nanoparticles; 0.5 W $m^{-2}$ 808 nm laser irradiation on BP@PLEL hydrogel can kill 99.5% of *S. aureus* colonies in 1 minute.[55] Also, in order to cope with bacterial resistance, Ag nanoparticle modified BP nanosheet (Ag@BP) nanohybrids were prepared. $Ag^+$ kills bacteria mainly by the oxidative dissolution mechanism, it can either destroy the bacterial cell membrane or strongly attract the sparse base of enzymatic proteins in bacteria at a very high concentration, and quickly bind together to reduce the activity of fine protozoan active enzymes, which show a strong antimicrobial effect.[75] $Ag^+$ release combined with the

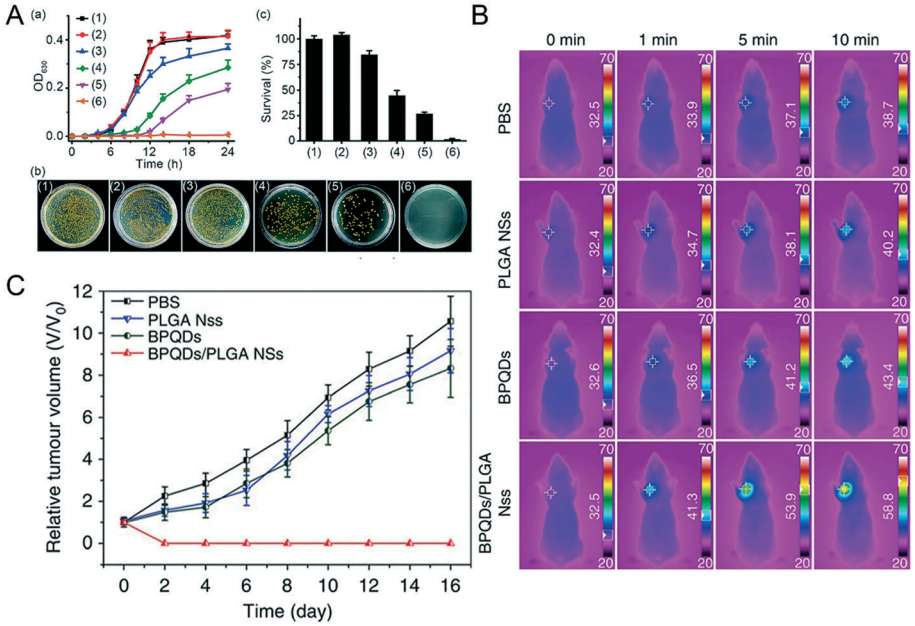


**Fig. 5** Photo-X therapies of NBP. A) Photothermal sterilization of NBP, (a) shows the growth curve of MRSA bacterial under the treatment of (1) blank control, (2) NIR, (3) BP, (4) Ag@BP, (5) BP + NIR, (6) Ag@BP + NIR, (b) is the images of MRSA bacterial colonies and (c) the corresponding quantitative analysis. Reprinted from Ouyang *et al.*[76] Copyright the Royal Society of Chemistry 2018. Infrared thermographic (B) and growth curves (C) of MCF7 breast tumor-bearing mice treated with different groups of PBS, PLGA NSs, BPQDs and BPQDs + NIR laser irradiation. Reprinted from Shao *et al.*[48] Copyright *Nature Communications* 2018.

photothermal effect of NBP showed the greatest inhibition effect at around 12–14 hours of incubation after being irradiated for 5 minutes (Fig. 5A).[76] Actually, bacterial infection can not only prevent wound healing, but also worsen the injury and lead to death of the organism. In this case, silk fibroin coated NBP (BP@SF) was used as a nanomedicine to treat the wound of injured mice, which significantly cleared the bacteria around the wound and promoted the growth and healing of wounded skin under NIR radiation.[77] Also, chitosan-coated BP nanosheets applied to the wounds of *S. aureus* ((1.0 × 107 CFU $mL^{-1}$)) infected mice can effectively accelerate the healing and scarring of wounds, because BP + NIR radiation triggers the phosphoinositide 3-kinase (PI3K), protein kinase B phosphorylation (Akt) and extracellular signal-regulated kinase (ERK1/2) signaling pathways, thereby enhancing cell proliferation and differentiation and accelerating the healing of wounds.[78]

**3.3.2 Photothermal therapy.** Photothermal therapy (PTT) is a new type of tumor treatment method that needs an excellent photothermal sensitizer and suitable laser irradiation. Since the black phosphorus nanomaterial is a single element of phosphorus and has good photothermal conversion characteristics in the near-infrared region, NBP is expected to be an excellent photosensitizer that can treat deep tumor sites since the penetration ability of the near-infrared light wave is stronger than that of visible light.[79] Wang *et al.* co-incubated HeLa cells with bare BPQDs directly followed by 808 nm laser irradiation of 1.0 W $cm^{-2}$ for 10 minutes and found that 100% of cancer cells were ablated at a concentration of 100 μM.[80] Similarly, Shao *et al.*[48] found that more than 10 ppm of BPQDs/PLGA could kill all the MCF7 and B16 cells under the same treatment. To this end, they tried to apply BPQDs/PLGA to tumor photothermal therapy in the body. After different concentrations of BPQDs and BPQDs/PLGA were injected into the MCF-7 tumor model BALB/c nude mice through the tail vein, the temperature on the tumor site was dynamically monitored for 10 minutes after injection (Fig. 5B), the temperature of tumors in mice of the BPQD treated group increased by around 10.8 degrees, while the temperature of tumors on the BPQDs/PLGA treated group increased by 26.3 degrees. After being irradiated with 808 nm near-infrared light multiple times within 48 hours post-injection, the tumors of the BPQDs/PLGA group disappeared gradually in 16 days post-injection and no recurrence occurred (Fig. 5C), while the tumors of the other groups were not effectively inhibited under the same treatment conditions. They hypothesized that the coating of PLGA greatly improved the stability of BPQDs *in vivo*, which prolonged the circulation time of BPQDs in blood, so that more BPQDs/PLGA could accumulate in the tumor part, and exert a better photothermal therapy effect. Coincidentally, treatment of breast cancer 4T1 tumor-bearing mice with PEGylated NBP with 808 nm laser irradiation (2.0 W $cm^{-2}$, 5 min) could induce tumor ablation and lengthen the life time of tumor-bearing mice.[81]

Furthermore, in order to improve the biological *in vivo* stability of BP nanomaterials as well as enhance the photothermal effect, some materials with biocompatibility and photosensitivity are used to modify the surface of BP nanomaterials. Previous reports show that the temperature of BP-Au NS could be increased from 25 °C to 70 °C within 5 minutes under 808 nm radiation (2 W $cm^{-2}$). During PTT, the temperature of the tumor site rapidly increased to achieve a

 

rapid photothermal treatment effect.[54] The cellulose/NBP hydrogel treated group showed better tumor inhibition and ablation than other control groups.[82] Moreover, NIR radiation can heat the BP-$SrCl_2$/PLGA microspheres and accelerate the release of $Sr^{2+}$ ions. The concentration of $Sr^{2+}$ between 8.76 and 87.60 mg $ml^{-1}$ can effectively promote osteogenic differentiation and enhance the repair ability of necrotic bones.[83,84] Surprisingly, BP@HA NFs associated with NIR laser significantly promote bone regeneration,[85] and BP and polyurethane (PU) can also be prepared as a shape memory polymer (SMP), which is near-infrared light-responsive with good biocompatibility, and may have great potential in biomedical applications such as self-expending stents.[86] However, in practical photothermal therapy applications, it is uncertain whether a higher temperature can give a better treatment effect. We also need to consider the patient's tolerance to pain, and reducing the pain of the patient, while maximizing the treatment effect is the most ideal.

**3.3.3 Photodynamic therapy.** Photodynamic therapy (PDT) is a non-invasive treatment that selectively kills tumor cells or other harmful cells with reactive oxygen species generated by photosensitizers.[87] Because of the hypoxic environment inside the tumor, it is critical to select photosensitizers that have good photosensitivity characteristics and biocompatibility. PDT of PEGylated BPQDs on S180 tumor-bearing mice effectively inhibited the tumor,[88] further confirming that BPQDs are a good choice as a photosensitizer. However, time point selection is quite important to improve the treatment effect of singlet $O_2$ dependent PDT; therefore, Liu *et al.* made a hybridized nanoplatform ($RMnO_2$-FBP) to realize a dual-model $O_2$ self-

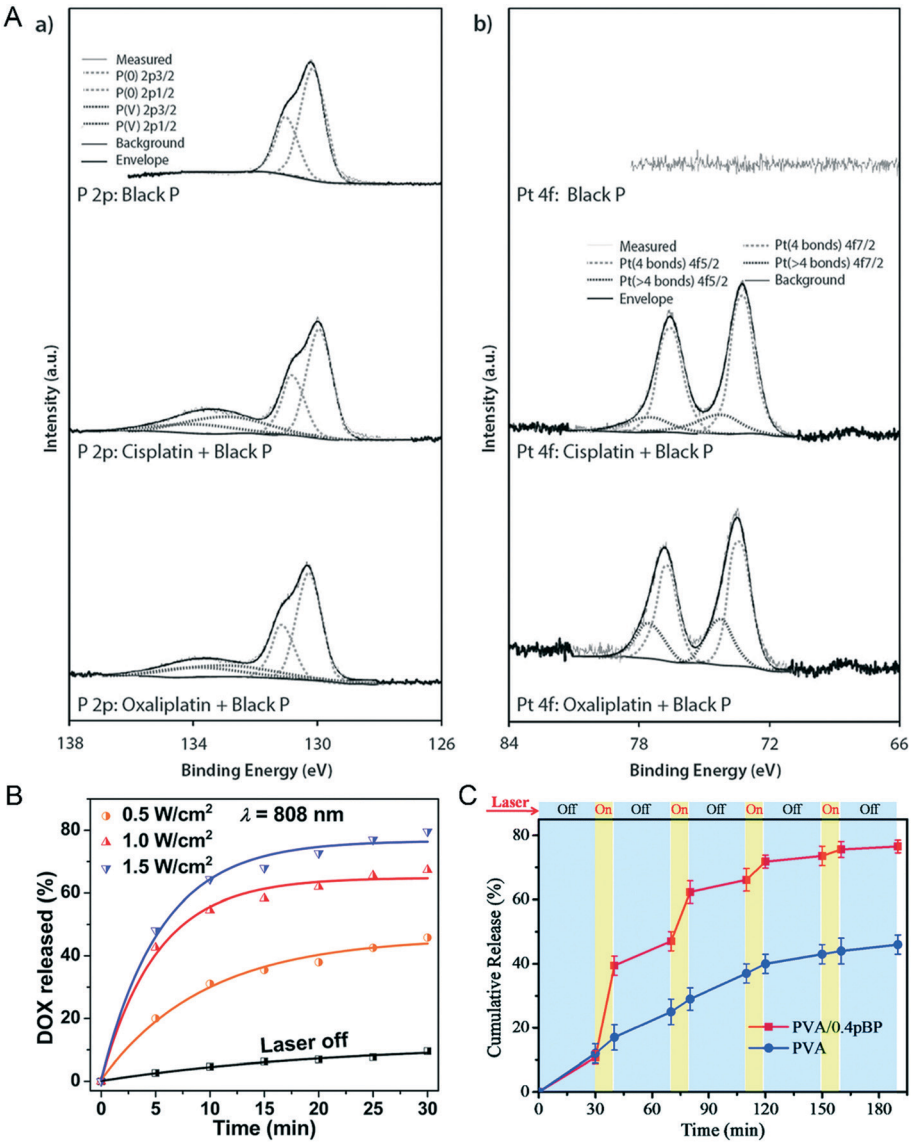


**Fig. 6** NBP loaded with an anti-tumor drug and light controlled release. A) XPS identification of of (a) cisplatin- and (b) oxaliplatin-bound black phosphorus. Reprinted from Fojtů *et al.*[17] Copyright 2017 WILEY-VCH Verlag GmbH & Co. KGaA, Weinheim. Light controlled switch of drug release from BPQD@Lipo (B)[49] and PVA/BP (C)[93] nanocarrier systems. B) Reprinted from Geng *et al.* C) Reprinted from Yang *et al.* Copyright the Royal Society of Chemistry 2018.

supply system, so that the optimal treatment time could be monitored through magnetic resonance imaging (MRI) and fluorescence imaging.[89] Yang *et al.* creatively prepared a BPs@Au@$Fe_3O_4$ photosensitizer which increased the singlet oxygen yield due to Au NPs and enhanced the MRI imaging because of $Fe_3O_4$ NPs.[90] Furthermore, stimuli-responsive NIR/ROS sensitive NBP vesicles (NBPVs) were prepared by Li *et al.*; by loading the cavity of NBPVs with an immunoadjuvant (CpG ODNs), they realized effective photodynamic immunotherapy in the tumor of mice.[91]

### 3.4 Drug delivery

Maintaining drug concentration within the therapeutic window concentration range is an important measure to overcome drug resistance.[92] In addition to its sensitive photonic response characteristics, another major feature of two-dimensional NBP is its enormous drug loading capacity due to its large specific surface area. Pumera *et al.* found that cisplatin and oxaliplatin can bind black P through Pt–P binding because the d electrons of metal Pt(II) can be effectively donated to the vacant d orbitals of P that can form a stable electron–hole pair. The distinct characteristic spectrum of Pt–P binding can be proved through X-ray photoelectron spectra (XPS) detection as shown in Fig. 6A.[17] Geng *et al.* designed a drug loading system using lipid-modified BPQDs (BPQDs@Lipo) with a drug encapsulation efficiency of 89.6%. This nanocarrier can realize drug-controlled release with a radiation switch, only less than 10% of DOX loaded in BPQDs@Lipo can be released without the use of NIR illumination, while almost 80% of the loaded Dox can be released after 1.5 W $cm^{-2}$ 808 nm light irradiation for 30 minutes, and the release efficiency is dependent on the intensity of the laser illumination (Fig. 6B).[49] Besides, Yang *et al.* used Congo red as a drug model and loaded it into PVA/pBP, after being irradiated by a 808 nm laser periodically (Fig. 6C); the release amount of Congo red in PVA/pBP was as high as 78%, more than twice the amount of drug released in the PVA group alone. It seems that NIR radiation causes BP to convert light energy into heat energy, and the internal temperature increase of PVA/pBP leads to PVA ablation, thus allowing more drugs to be released.[93] Apparently, the drug loading ability of NBP smartly reduces the side effect of a chemotherapy drug in anti-tumor therapy, especially after a further targeted modification. A previous study reported that PEGylated NBP coupled with the target molecule folic acid (FA) was loaded with DOX to form a DOX-loaded BP-PEG-FA targeted drug delivery nano-system.[94] After they were injected into the tumor-bearing mice through the tail vein for 24 hours, the tumor was locally radiated with a 808 nm laser with an intensity of 1 W $cm^{-2}$ for 10 minutes. They found that the tumor volume of the BP-PEG-FA/DOX NSs + NIR treated group significantly shrank compared with that of the control group at 14 days post-radiation, which showed the best healing effect compared with any other groups.

In addition to the loading of chemotherapy drugs for antitumor therapy, NBP can also be loaded with gene fragments to realize gene therapy. Yin *et al.* modified BPQDs (BPQDs@PAH) with a polyelectrolyte polymer, and then loaded them with LSD1 siRNA to prepare the BPQDs–LSD1 siRNA complex. Under near-infrared light irradiation, the BPQDs–LSD1 siRNA complex endocytosed into human ovarian teratoma PA-1 cells, which exhibited a higher transfection efficiency than commercially available agents such as lipo2000 and Oligo. The release of LSD1 siRNA significantly inhibited the expression of LSD-1 mRNA in PA-1 cells, and further effectively inhibited the proliferation of PA-1 cells by 80%.[95] It was also confirmed that NBP can be used as a nano-carrier to deliver gene Cas9N3 into MCF7 cells to achieve gene editing.[96] Excitingly, the photothermal effect of BP also improves the permeability of the blood–brain barrier, making it possible to treat neurological diseases with BP-loaded drugs.[38,97] Thus, drug loaded NBP modified with suitable functionalized materials or structures can be an excellent drug delivery nanocarrier in realizing disease targeted therapies.

## 4 Toxic assessment of NBP

### 4.1 *In vitro* nano–bio interactions of NBP

When exogenous nanomaterials interact with living biological samples, nano–bio interactions would immediately take place and affect the body to respond at the cellular and molecular level.[98] NBP has attracted great attention from the bioengineering community due to its potential applications in imaging and targeted drug delivery. But its biosafety has raised many concerns and thus it greatly limits its use in clinical research.[99–101] This section summarizes the nano–bio interactions of NBP *in vitro* and *in vivo*.

**4.1.1 Interaction between the cell membrane and NBP.** It was reported that NBP induced apoptosis in L-929 fibroblastic cells by causing membrane disruption.[102] NBP with a lateral size of 960 ± 303 nm and a thickness of 6.8 ± 0.58 nm was found to increase lactate dehydrogenase (LDH) release from L-929 fibroblastic cells. LDH is an enzyme that exists solely in the cytoplasm, which can only be detected in the extracellular environment when the cell membrane ruptures, and it is regarded as an effective indicator to evaluate the integrity of cell membranes.[103] After the cells were treated with 16 μg $mL^{-1}$ of NBP for 24 hours, the LDH release rate was 1.4 times higher than that of the control group (Fig. 7A). A similar nano–bio interaction phenomenon was discovered in the case study of *E. coli* and *B. subtilis* treated with NBP.[72] Xiong *et al.*[104] found that NBP was able to kill Gram negative *E. coli* after 6 hours of treatment and it resulted from the disruption of membrane integrity (Fig. 7B). Thus, the loss of cell membrane integrity is the main driving force to induce the cell apoptosis process. However, BP with nanoscale particle sizes did not appear to promote apoptosis in cells.[80] We speculate that there is a critical size effect for adverse nano–bio interactions of NBP to take place. Zhang

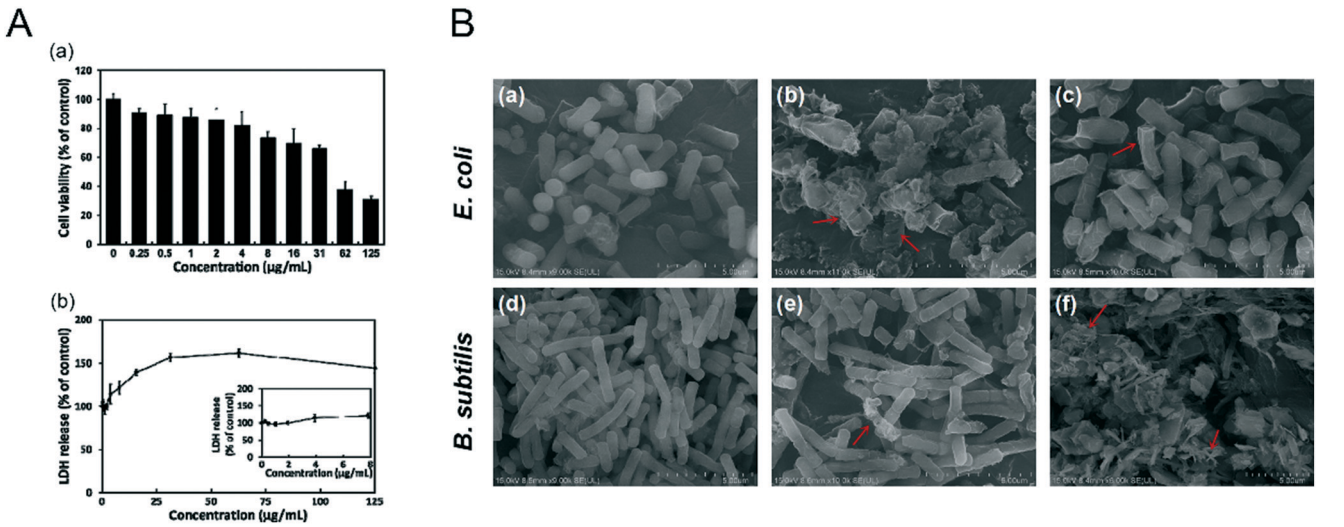


Fig. 7 Bio–nano interaction between the cell membrane and NBP. A) Cell viability (a) and LDH release (b) of L-929 fibroblasts after 24 h treatment of layered BP. Reprinted from Song *et al.*[102] Copyright the 2018 nanomaterials. B) SEM images of *E. coli* (a–c) and *B. subtilis* (d–f) under the treatment of 0 μg $mL^{-1}$ (a and d) and 100 μg $mL^{-1}$ (b and c, e and f) of NBPSs after 6 h (b and e) and 12 h (c and f). Reprinted from Xiong *et al.*[104] Copyright the 2018 Elsevier Inc.

*et al.*[105] employed a zwitterionic 1,2-dioleoylsn-*glycero*-3-phosphocholine (DOPC) vesicle-based lipid membrane to detect the membrane integrity under exposure to different sizes of BPNSs. It was found that BPNSs with large sizes (884.0 ± 102.2 nm) caused severe disruption to the membrane integrity, while smaller ones (425 ± 78.8 nm and 208.5 ± 46.9 nm) did not. Some studies were also performed to investigate the effects of 2D nanomaterials on the cell membrane. Zhou *et al.* reported the impact of graphene on the cell membrane of *E. coli*. During the co-incubation of graphene with *E. coli*, graphene was found to be trapped within the membrane lipids due to the strong van der Waals and hydrophobic interactions from the cell membrane since they are made of long alkyl-chain phospholipid molecules.[106] When graphene was contained within the membrane lipids, it could penetrate the lipid bilayer within several nanoseconds. During this process, a fraction of the phospholipid molecules attached themselves to the graphene surface, which resulted in the deformation and disruption of the cell membrane.[107] Interestingly, NBP shows a similar effect, and Guo *et al.* revealed that the sharp edge of the BP nanosheet can physically disrupt the membrane of bacteria and cause RNA leakage, which induced the death of bacteria.[108] Another study found that human serum album (HSA) functionalized BP nanosheets displayed little toxicity to U87MG cells. The viability of U87MG cells was higher than 80% even when they were treated with 500 μg $ml^{-1}$ of HSA functionalized BP nanosheets for 24 hours.[50] It is safe to conclude that surface modification of NBP is required for reducing cell membrane disruption during *in vitro* and *in vivo* applications.

**4.1.2 Effect on cellular function after NBP exposure.** In addition to cell membrane integrity disruption, NBP also generates reactive oxygen species (ROS) and causes organelle dysfunction in several ways. In the absence of any surface modification, NBP can easily oxidize and degrade;[74] also ROS is generated when it is exposed to visible light.[44] Basically, the electron transfer between P and the ground state oxygen form serves as a platform for the production of ROS.[12] It was found that NBP induced a significant increase of ROS generation ($P < 0.001$) when it was incubated with *E. coli* and *B. subtilis*.[44] It was clear that the concentration level of ROS was time- and dose-dependent of NBP exposure.[109,110] However, there is no evidence to prove that the ROS generation is related to the lateral size of NBP.[105] As previously mentioned, bare BPQDs not only caused a significant increase of 3,4-methylenedioxyanphetamine (MDA), but also decreased the catalase (CAT) level in the liver of mice one day post-injection.[28] MDA is the product of cellular lipid peroxidation and over production of MDA promotes the generation of ROS. Superoxide dismutase (SOD) and CAT are antioxidant enzymes, and ROS such as superoxide radicals ($O_2^-$) can be catalyzed to form molecular oxygen ($O_2$) and hydrogen peroxide ($H_2O_2$) which can be further broken down into $H_2O$ by CAT.[111] In other words, ROS can effectively damage the functions of the cell and its organelles by oxidizing phospholipid molecules in the bilayer structure.

Yu and Jiang *et al.* reported that BPQDs can significantly reduce the ATP content after their uptake by macrophage Raw 264.7 cells. After the cell uptake ability was inhibited by cytochalasin D (CytD), an inhibitor of classical actin polymerization on cell uptake, the ATP content level was significantly enhanced compared with that of the BPQD treated group without CytD pretreatment (Fig. 8).[112] This means that the uptake of BPQDs disturbed the secretion of ATP. It is noteworthy that there are a lot of polyunsaturated fatty acids (PUFAs) in the biological membrane which are vulnerable to the attack of

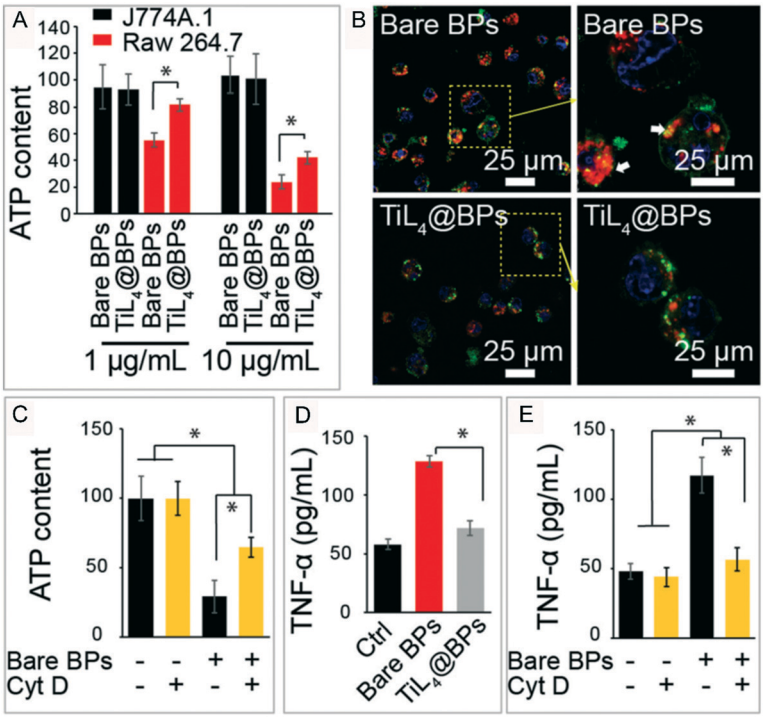


Fig. 8 ROS induced by NBP disordered cell functions. ATP metabolism (A and C), the morphology of lysosome (B) and TNF-α. Cytokine excretion (D and E) of macrophages under the treatment of bare BP and $TiL_4$@BP, * indicates $p < 0.05$. Reprinted from Qu *et al.*[112] Copyright 2017 The Authors. Published by Wiley-VCH Verlag GmbH & Co. KGaA, Weinheim.

free radicals. Lipid oxidation produces MDA that results in the functional and metabolic disorder of cells. As the energy pump of cells, the mitochondrion plays the most important role in ATP production.[113] With the increase of intracellular ROS brought in by the invasion of BPQDs, lipids in the mitochondrial membrane get oxidized and the membrane potential of mitochondria is compromised, which affected the ATP metabolism of mitochondria that induced cell apoptosis.[110] In addition to the mitochondria, the lysosome macrophages (J774A.1 cells) in the BPQD treated group were also more swollen than those in the control group,[112] and a similar effect can also be caused by 2D $MoS_2$ nanosheets.[114] Here we speculated that there are two causes of the swollen lysosomes. First, some of the invading BPQDs were swallowed by the lysosomes. Second, BPQDs induced oxidative damage and even death of some organelles which were further cleared by the lysosomes. Beyond that, ROS can activate caspase-3, a key enzyme in the apoptosis process, and trigger the apoptotic response.[115] The activation of caspase-3 can cause a programmed death of cells.[116] Almost 65% of caspase-3 was activated under 100 μg $ml^{-1}$ NBP treatment for 48 hours.[110] From these points, we can conclude that ROS generation is a key factor in cell dysfunction and apoptosis.

**4.1.3 Cellular fate after NBP exposure.** The viability and proliferation of cells are always evaluated through 3-(4,5-dimethyl-2-thiazolyl)-2,5-diphenyl-2-*H*-tetrazolium bromide (MTT), cell counting kit-8 (CCK-8) and 3-(4,5-dimethyl-2-thiazolyl)-5-(3-carboxymethoxypheny)-2-(4-sulfophenyl)-2*H*-etrazolium, inner salt (MTS) assays. The mitochondrial activity of cells is a sensitive parameter in reflecting the cell viability. The MTT/CCK-8/WST-8 molecule can be reduced to a kind of product such as formazan with the proliferation of cells by the amber dehydrogenase of the mitochondria in living cells. Cell viability is calculated by quantifying the reduced product through optical absorbance measurement. Here, we have summarized the cytotoxicity of different NBPs on different cell lines under a variety of detection assays (Table 1). As for the cytotoxicity of BPQDs and NBP, previous reports revealed that the viability of HeLa cells is no less than 90% even after being incubated with ultra-small BPQDs at a concentration of 0.5 mg $ml^{-1}$ for 48 hours[80] and BPNSs at a concentration of 0.1 mg $ml^{-1}$ for 72 h.[27] The viability of MDA-MB-231 cells treated with ultrathin NBP (2 nm of height) for 4 hours at the highest concentration of 0.2 μg $ml^{-1}$ is stable in a normal range.[56] To clarify the relationship between the size of BP nanomaterials and cytotoxicity, three types of BPNSs varying from lateral sizes and thicknesses called BP-1, BP-2 and BP-3 were prepared to test their cytotoxicity.[105] After being incubated with mouse fibroblasts (NIH-3T3), human colonic epithelial cells (HCoEpiC) and human embryonic kidney cells (293T) to test their cytotoxicity, BPNSs with the largest size showed the most severe toxicity while the smallest sized NBP showed a moderate toxic effect (Fig. 9A). From this point, it is clear that

 

**Table 1** Cytotoxicity of different sized NBP

| Type of NBP | TEM/DLS | Cell line | Assay indicators | Effect | Ref. |
|---|---|---|---|---|---|
| NBPS | Hydrodynamic diameter: 960 ± 303 nm | L-929 | CCK-8 kit | Viability is around 37% at the concentration of 62 μg $ml^{-1}$ for 24 hours | 102 |
| BPQD | — | J774A.1 | ATP assay | ATP content was significantly decreased to around 50% at 1 μg $ml^{-1}$ treatment for 12 hours, dose and time dependent | 112 |
| BPQD | — | Raw 267.4 | ATP assay | ATP content stayed normal at 1 μg $ml^{-1}$ treatment for 24 hours | 112 |
| NBPS | Diameter: 884.0 ± 102.2 nm Thickness: 91.9 ± 32.0 nm | NIH3T3, HCoEpiC, 293T | Real-time cell analysis | $IC_{50}$ value is 3.93, 47.31 and 1.52 μg $ml^{-1}$ of NIH3T3, HCoEpiC and 293T, respectively, 24 hours treatment, dose dependent | 105 |
| NBPS | Diameter: 425.5 ± 78.8 nm Thickness: 27.0 ± 12.0 nm | NIH3T3, HCoEpiC, 293T | Real-time cell analysis | $IC_{50}$ value is 8.15, 175.13 and 7.10 μg $ml^{-1}$ of NIH3T3, HCoEpiC and 293T, respectively, 24 hours treatment, dose dependent | 105 |
| NBPS | Diameter: 208.5 ± 46.9 nm Thickness: 17.4 ± 9.1 nm | NIH3T3, HCoEpiC, 293T | Real-time cell analysis | $IC_{50}$ value is 44.51 and 63.72 μg $ml^{-1}$ of NIH3T3 and 293T, respectively, $IC_{50}$ value of HCoEpiC cannot be detected under the highest dosage, 24 hours treatment, dose dependent | 105 |
| L-NBPS | Diameter: 394 ± 75 nm Thickness: 16.50 ± 1.27 nm | LO2 HeLa MCF-7 | CCK-8 | Viability of all cell lines is higher than 80% under the highest concentration of 50.0 μg $ml^{-1}$ for 48 hours | 122 |
| M-NBPS | Diameter: 118 ± 22 nm Thickness: 6.07 ± 0.21 nm | LO2 HeLa MCF-7 | CCK-8 | Viability of all cell lines is higher than 80% under the highest concentration of 50.0 μg $ml^{-1}$ for 48 hours | 122 |
| S-NBPS | Diameter: 4.5 ± 0.6 nm Thickness: 2.27 ± 0.21 nm | LO2 HeLa MCF-7 | CCK-8 | Viability of all cell lines is higher than 80% under the highest concentration of 50.0 μg $ml^{-1}$ for 48 hours | 122 |
| NBPS | Diameter: several hundred nanometers Thickness: 4.0 ± 1.0 nm | LO2 | MTT, Live/Dead staining assay | Viability of all cell lines is higher than 80% under the highest concentration of 2.0 mg $mL^{-1}$ for 48 hours | 44 |
| BPQDs | Diameter: 2.7 ± 0.7 nm Thickness: 1.5 ± 0.8 nm | HeLa | Annexin V-FITC/PI staining | Viability of cell is 36% under 200 μg $mL^{-1}$ for 24 hours, ROS content increased with increasing dose | 28 |
| NBPS | Diameter: several hundred nanometers Thickness: ~2.0 nm | MDAMB-231 | MTT | Little effect on the cell viability in the dark in the highest concentration of 2.0 μg $ml^{-1}$ for 4 hours | 56 |
| BPQD | Diameter: 2.1 ± 0.1 nm | RBCs | Morphology | Morphology of the RBCs stayed normal under the 0.1–0.5 mg $ml^{-1}$ treatment for 24 hours | 80 |
| NBPS | Diameter: 208.2 ± 10.6 nm Thickness: ~5 nm | HeLa | MTT | Viability is higher than 90% under 100 μg $ml^{-1}$ treatment for 48 hours | 27 |
| NBPS | Hydrodynamic diameter: 164 ± 24 nm | C2C12 | CCK-8 | Viability is ~ 30% and lower than 20% under 250 μg $ml^{-1}$ treatment for 24 h and 48 h, dose- and time dependent | 81 |
| NBPS | — | NIH3T3 | LIVE/DEAD staining assay | Viability is ~60% when treated with a concentration of 100 μg $ml^{-1}$, <10% at concentration of 200 μg $ml^{-1}$ | 123 |
| BPQDs | Diameter: ~10 nm Thickness: ~8 nm | HeLa COS-7 CHO-K1 | MTT | Viability is no less than 90% under the highest concentration of 1 mg $mL^{-1}$ for 12 hours | 26 |
| BPQD | Diameter: 3.3 ± 0.6 nm | HeLa $LO_2$ | MTT | Viabilities of all cell lines are higher than 90% under the highest concentration of 40.5 μg $ml^{-1}$ for 24 hours | 88 |
| NBPS | — | A549 | MTT & WST-8 | Viabilities are 34% (MTT) and 48% (WST-8) at 50 μg $ml^{-1}$ exposure for 24 hours | 119 |
| NBPS | Diameter: ~200 nm | 4T1 HUVEC U251 LLC | CCK-8 AM/PI staining | Viabilities of all cell lines are higher than 95% at the highest dosage 100 μg $ml^{-1}$ exposure for 72 hours | 97 |
| NBPS | Diameter: ~500 nm Thickness: 5.3–5.9 nm | BEAS-2B | MTT Annexin V-FITC/PI apoptosis assay | Viability is reduced from 80% (24 h) to 38% (48 h) under 100 μg $ml^{-1}$ treatment, reduced from almost 85% to 38% with the increase of dosage from 50 μg $ml^{-1}$ to 100 μg $ml^{-1}$ for 48 hours, ATP is decreased and also time- and dose-dependent | 110 |
| BP flakes | Diameter: ~2 μm Thickness: 5–10 nm | NIH3T3 nHDF HT1080 | CCK-8 | Viabilities of all cell lines are time- and dose-dependent | 124 |

the cytotoxicity response of NBP is size dependent. This result is unlike that of 2D $MoS_2$; although the cytotoxicity of $MoS_2$ is size dependent, it is the smallest lateral size that induces the most severe toxic effect.[117] Another kind of two-dimensional (2D) nanomaterial, graphene oxide (GO), was also discovered to induce cytotoxicity because of the direct reaction with the cell membrane.[118]

Although many of the reports showed that NBP is compatible in the biological environment under some certain dosages, some argue about this conclusion. Xing *et al.* found that bare NBP significantly reduces the viability and proliferation of mammalian cell lines such as NIH3T3, HCoEpiC and 293T and causes apoptosis of these cell lines. According to Fig. 9B, intracellular ROS generation in NBP treated groups is around ten-fold higher than that of the control group. This means that the existence of NBP caused ROS generation and led to cell apoptosis.[105] Also, compared to BPNSs, BPQDs are easier to be endocytosed into the cell without disruption of membrane integrity, but they can induce cell apoptosis by ROS generation that is dose-dependent as well.[67] Interestingly, Prof. Martin Pumera and his team revealed that BP could reduce the MTT assay reagent into insoluble formazan during the MTT test, which interferes with the absorbance measurement and the cell viability is overestimated.[119] This is mainly because P is easily oxidized and the MTT reagent is easily reduced, so the coincubation of these two makes the redox reaction easily occur. If this does happen, the addition of NBP may influence all these kinds of viability test assays with the same detection principle. For improving the biocompatibility of NBP, a variety of innovative approaches for surface modification have been tried to reduce its biological toxicity. Since P is easy to be oxidized, materials such as polyethylene glycol (PEG), poly(lactic-*co*-glycolic acid) (PLGA), titanium sulfonate ligand ($TiL_4$), liposomes and so on are used for NBP functionalization. Many reports verified that the biocompatibility of BPQDs improved a lot after being layered with PEG;[47,81,120] the MTT tested viabilities of 293T, C6, MCF7 and HSC cell lines were higher than 80% after being incubated with PEGylated BPQDs at a concentration of 200 μg $ml^{-1}$ for 48 hours.[33] Moreover, NBPs modified with PEG exhibited little side effect on HeLa cells as well.[53,94] This suggested that the existence of PEG on the surface of NBP protects the core from being oxidized and further reduces the bio-interaction between nanoparticles and cells. Besides, modification using polymer materials and bio-materials also made NBP more stable in biological environments and more biocompatible when it was used in theranostic applications.[121] This further confirmed that surface functionalized NBP is safer than the bare ones.

### 4.2 *In vivo* toxicity assessment of NBP

It is well known that the retention and metabolism of nanomaterials in organisms play a great role in biosafety assessment of nanomaterials. If the invasive exogenous nanoparticles cannot be excreted out of the body, nano–bio interactions between nanoparticles and organs are inevitable since the exogenous materials always accumulate in the liver and spleen due to the reticuloendothelial system (RES). The nanoparticles, such as metal quantum dots,[22] semiconductor quantum dots,[125] polymer quantum dots, *etc.*,[126] have been reported to be mainly distributed in the liver, spleen and kidney after entering the mice. Other studies revealed that the average body weight displays a downward trend in the first week after injection of NBP, but it returns to normal levels in the following month as compared to that of the untreated group,[80] and studies confirmed that the nano–bio interactions between NBP and *in vivo* organisms are the main causes of this phenomenon.[127,128]

**4.2.1 Toxic effect of NBP on blood circulation.** The blood circulatory system connects the whole body, thereby it must be quite sensitive in responding to the invasion of nanomaterials. Differential count of blood cells and some protease levels in the blood are common indicators to assess the health condition of an individual. Zhao and Wei *et al.* added bare BPQDs and NBP into the whole blood of mice to simulate the potential nano–bio interactions between NBP and the blood circulatory system.[45] They found that a lot of plasma proteins attached themselves to the surface of BPQDs and BPNSs to form NBP–corona complexes including the BPQD–corona complex and BPNS–corona complex, which changed the hydrodynamic diameter of BPQDs and BPNSs from 5.6 ± 1.2 nm and 338.4 ± 2.3 nm to 362.5 ± 5.6 nm and 365.3 ± 5.9 nm, and refined the morphology of BPQDs from ultra-small nanosheets to spherical nanoparticles. Previous reports declared that plasma proteins can adhere to the surface of nanoparticles as soon as they are exposed to the nanoparticles.[129] In this study, the zeta potential of BPQDs and BPNSs was reduced from −20.6 mV and −18.1 mV to −7.8 mV and −13.7 mV after their entry into the whole blood, which implied that plasma proteins attached themselves to the surface of BP nanoparticles in a short time (Fig. 10A). We speculated that the negatively charged BP nanoparticles mainly attracted the positively charged proteins,[45] but further analysis showed that almost 62.00% and 64.93% of proteins that attached to the BPQD–corona complex and BPNS–corona complex were negatively charged. From this aspect, it can be concluded that charge absorption may not be the main driving force during the reaction between BP nanoparticles and plasma proteins.

According to the results of research done by Mu *et al.* (Fig. 10B), the half lifetime of bare BPQDs is 0.8 hours during blood circulation; after intraperitoneal injection of 200 μL of 1.7 mg $mL^{-1}$ BPQDs, globulin (GLOB) in the blood of male C57BL/6 mice gave a sharp increment one day post-treatment ($P < 0.05$) and then recovered after one week, while the level of glucose (GLU) dropped sharply from 3.4 mmol $L^{-1}$ (control group) to 1.4 mmol $L^{-1}$ in 24 hours, but gradually returned to normal levels one month post-injection. The drop in the GLU level could be related to the weight lost on the first day after treatment. Other abnormal biochemical indicators such as

 

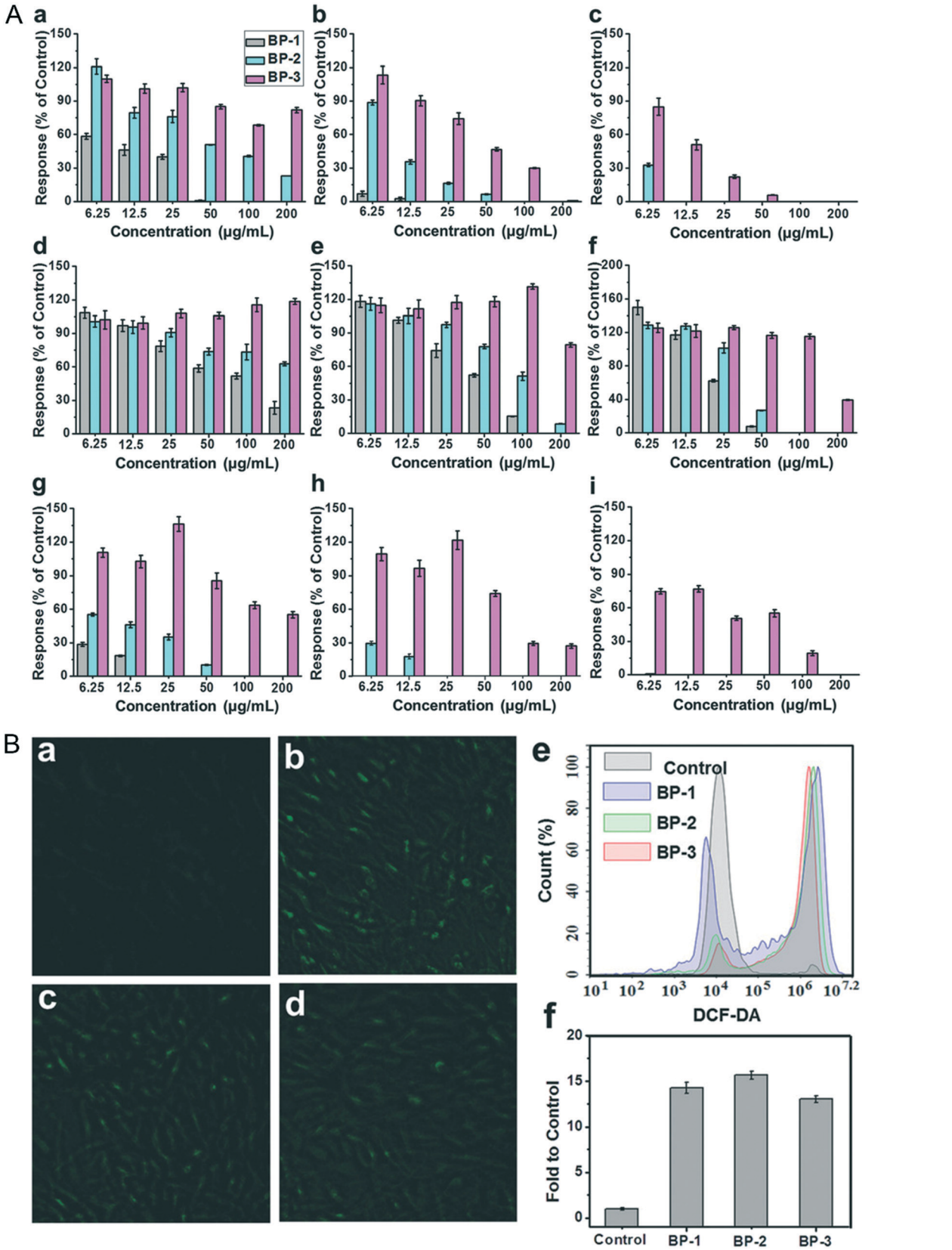


**Fig. 9** A) Percentage of cell responses of different cell lines: NIH3T3 (a–c), HCoEpiC (d–f), and 293T cells (g–i), after 12 h, 24 h and 48 h of exposure to layered BP. B) Intracellular ROS detection of NIH3T3 cells exposed to 10 μg $mL^{-1}$ of layered BP for 4 h *via* DCF-DA staining: a) control, b) BP-1, c) BP-2, and d) BP-3; e and f) fluorescence intensity and flow cytometry analysis. Reprinted from Zhang *et al.*[105] Copyright 2017 Wiley-VCH Verlag GmbH & Co. KGaA, Weinheim.

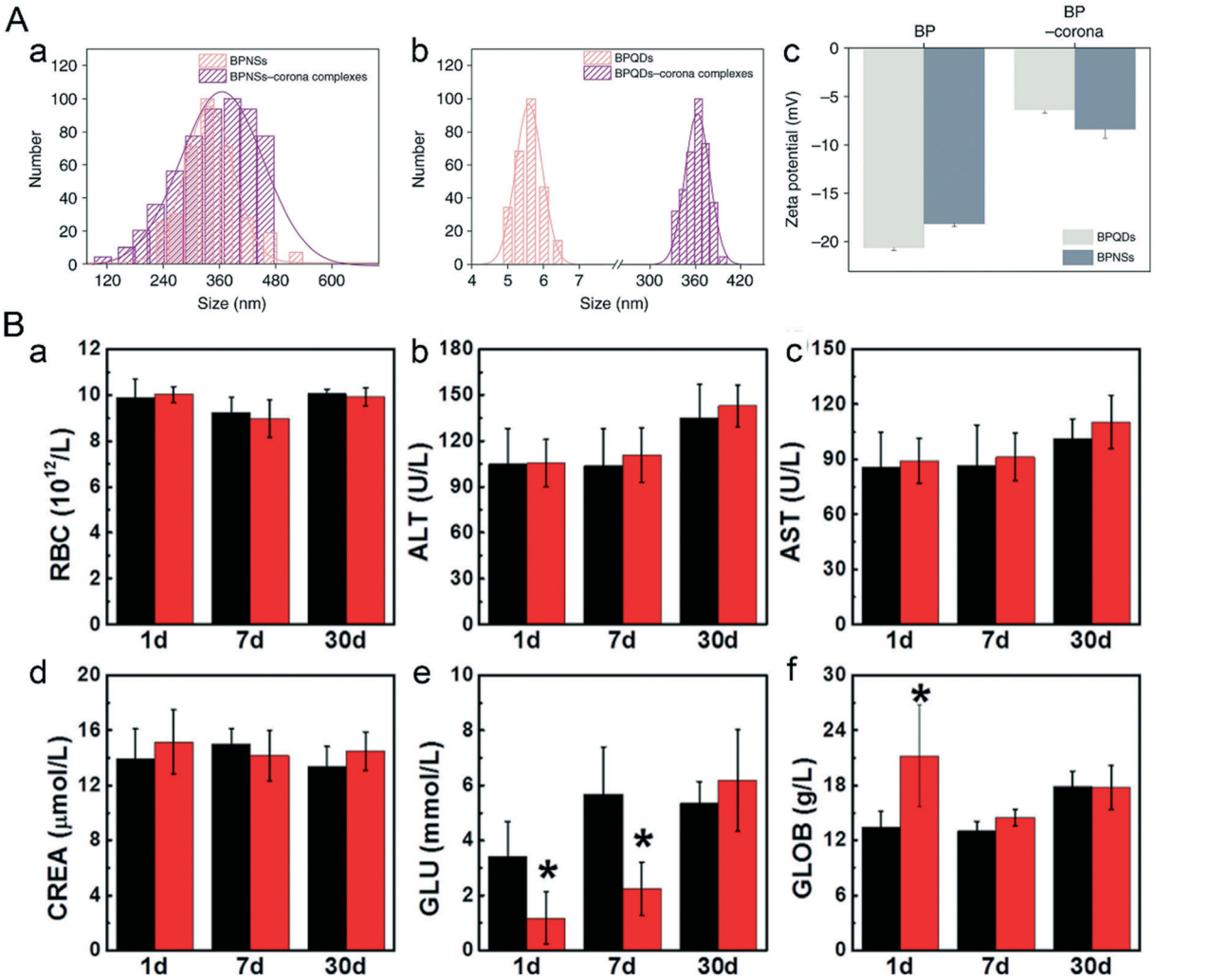


**Fig. 10** Nano–bio interaction between bare NBP and the blood circulatory system. A) Hydrodynamic sizes (a and b) and zeta potentials (c) of BP and BP–corona complexes. Reprinted from Mo *et al.*[45] Copyright the 2018 *Nature Communications*. B) Hematological data like the count of (a) RBC and blood chemistry analysis including (b) ALT, (c) AST, (d) CREA, (e) GLU, (f) GLOB of mice after BPQD treatment. Reprinted from Mu *et al.*[28] Copyright the 2017 American Chemical Society.

RBC count, liver function parameters (ALT, AST) and renal function parameters (CREA, BUN) also went back to normal levels in 30 days post-injection.[28] For assessing the potential vascular risk of NBP, Chen *et al.* examined the aortic structure of C57BL/c mice after being injected intravenously with 100 μg $mL^{-1}$ NBP dispersion (100 μL) for 1 day and 7 days, respectively. The results showed no difference in aortas, but the transcriptome aberration of mouse aortas might trigger abnormal vasoconstriction.[130] However, after bare NBP was modified by some surface functional materials, the hemotoxic effect changed a lot. When 7.1 mg $kg^{-1}$ of PEGylated NBP was intravenously injected into BALB/c mice, there was no influence on mouse blood hemogram indicators in 1 day, 7 days and 14 days post-injection.[94] Similarly, 0.2 mg PLGA-encapsulated BPQDs (BPQDs/PLGA) were biocompatible when they were injected into the blood circulation system of mice for 1 day, 7 days and 28 days.[48] All the results above show that certain specific amounts of BPQDs can cause short term hemotoxicity in an organism which gradually becomes better as time passes. The cause of *in vivo* hemotoxicity of NBP requires further investigation, but one thing can be surely said, that is, surface modification greatly improves the stability of BP nanomaterials, thereby effectively improving the biocompatibility of BP nanomaterials and mitigating their toxic effect.

**4.2.2 Immunological toxicity of NBP.** Compared to the *in vitro* surroundings, the *in vivo* environment is much more complicated. Almost 70% of the NBP bound proteins in the blood circulatory system are immune relevant proteins, and some of these immune system proteins play the role of opsonin which labels nanoparticles as foreign invaders that can attract phagocytes like macrophages and neutrophils, leading to swallowing of these invasive nanoparticles by phagocytosis (Fig. 11A). It has been confirmed that BP–corona complexes interact with stromal interaction molecule 2 (STIM2) inducing $Ca^{2+}$ influx, which further induces the activation of p38 and NF-κB and causes the polarization of M0 macrophages to M1 macrophages.[131] The NF-κB pathway

 

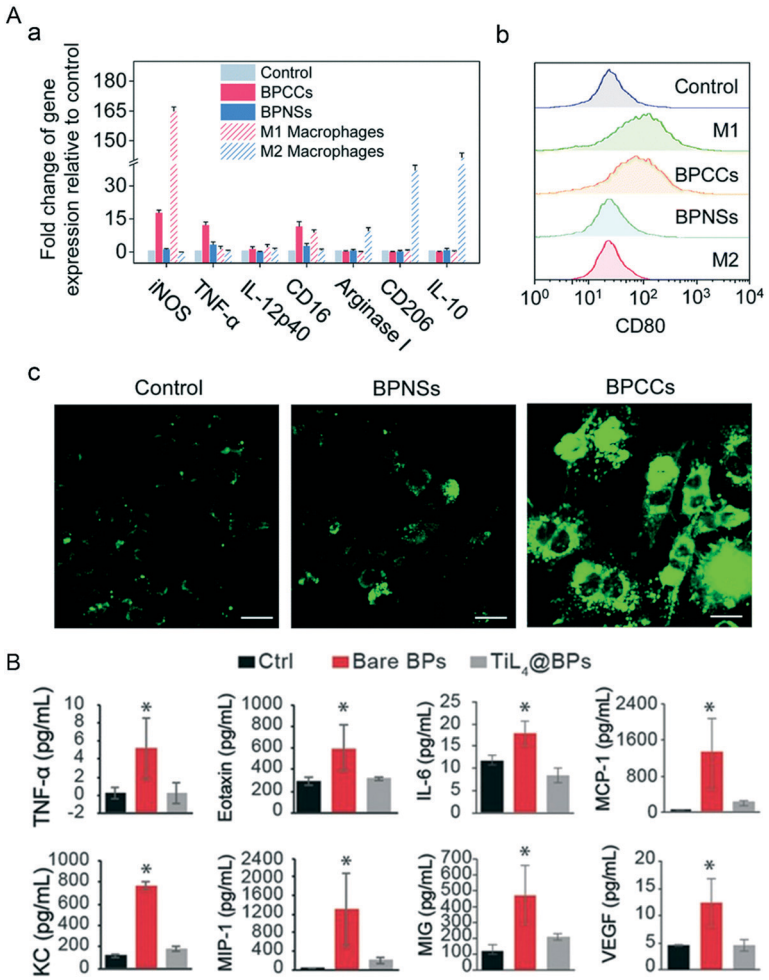


**Fig. 11** Macrophage polarization and inflammation response induced by the invasion of NBP. A) Changes of mark gene levels (a and b) of M1 and M2 macrophages after BP–corona complex (BPCC) treatment. (c) Intracellular $Ca^{2+}$ concentration in macrophages stained with Fluo-4 AM after NBPS and BPCC treatment. Reprinted from Mo *et al.*[131] Copyright the Royal Society of Chemistry 2020. B) Levels of inflammatory cytokines in mouse serum 1 d post-treatment of PBS (Ctrl), bare BPs and $TiL_4$@BPs, $*p < 0.05$. Reprinted from Mu *et al.*[28] Copyright the 2017 American Chemical Society.

plays an essential role in inflammatory reactions,[132] that is why the levels of proinflammatory cytokines such as IL-1ß, IL-6, IL-8. IL-9 and IL-10 rise significantly. Besides, exposure to bare BPQDs caused DNA damage of bone marrow nucleated cells (BMNCs) collected from bilateral femurs of mice after 1-day treatment. BMNC is a kind of macrophage that plays a critical role in hematopoietic function, and its reduction may weaken the hematopoietic capacity in mice. Exhilaratingly, the DNA damage and the decrease of BMNCs recovered on days 7 and 30 respectively post-injection, which means that the resulting damage caused by BP exposure is temporary and the organism can recover by itself.[28]

Additionally, intravenous injection of 500 μg $kg^{-1}$ of bare BPQDs into BALB/c mice induced a dramatic increase of neutrophils in peripheral blood, and cytokines including TNF-α, eotaxin, IL-6, MCP-1, KC, MIP-1, MIG-1 and VEGF in serum were significantly increased as well (Fig. 11B). Moreover, immune cells (F4/80+/+monocytes/monocyte) were recruited in a large number (31.4%) by the spleen after the invasion of bare BPQDs, even more than twice of the level of the control group (15.1%), which means that the accumulation of BPs in the spleen can induce serious inflammation. Gratifyingly, BP modified with $TiL_4$ ($TiL_4$@BP) has not caused any significant difference in all the indicators detected above compared to those of the control group, mainly because the modified $TiL_4$ effectively improved the stability of BP and limited the reaction of BP with the surrounding oxygen, thereby avoiding the occurrence of inflammatory stress *in vivo*.[112] Other biocompatible modification materials such as cellulose also work in reducing the toxicity of NBP, and cytokines including TNF-α, IL-1 and IL-6 in the serum of C57BL/6 mice were in a healthy range after being subcutaneously injected with 380 ppm cellulose@NBP.[77] So, although the toxic effects brought by the invasion of bare NBP can be eliminated by the immune system of the living body itself, it is better to do some biocompatible functionalization of NBP when it is used in biomedical applications.

**4.2.3 Nephrotoxicity of NBP.** The study of Shao *et al.* discovered that BPQDs modified with PLGA (BPQDs/PLGA) and coupled with the fluorescent molecule Cy5.5 can aggregate in the liver, spleen and kidney of tumor-bearing mice after tail vein injection.[48] Recently, NBP was found to cause nephrotoxicity in mice. He *et al.*[133] revealed that bare NBP with a hydrodynamic size of 15.1 ± 1.8 nm induced a significant toxic effect on the kidney of BALB/c mice after being intragastrically administered with 1 mg $kg^{-1}$ $bw^{-1}$ $d^{-1}$ NBP for 7 days. After the treatment, the uric acid (UA) content and creatinine content in the serum of mice were significantly increased and decreased, respectively (Fig. 12). The histology staining of kidney tissues displayed that NBP exposure caused the increment of neutrophils and degeneration of tubules, which indicated that NBP invasion disrupted the structure of the kidney. What's more, NBP was found to increase the serum adiponectin level (from 8.21 mg $L^{-1}$ to 10.32 mg $L^{-1}$) and decrease the serum leptin level (8.87 mg $L^{-1}$ to 7.60 mg $L^{-1}$) significantly. According to previous studies, adiponectin is a adipokine related to glucose uptake and insulin sensitivity,[134] leptin is another adipokine related to insulin sensitivity and kidney disease,[135] and the leptin/adiponectin ratio is considered a diagnostic biomarker of kidney disease since it is positively associated with insulin insensitivity.[136] In the study of He *et al.*, the value of the leptin/adiponectin ratio was decreased significantly after NBP treatment compared with the negative control group. And the expression of IRα, IRS1, IRS and AKT, proteins involved in the insulin response process, was significantly decreased in kidney tissues. Besides, they also found that NBP can also upregulate the expression of endoplasmic reticulum (ER) stress markers GRP78, IRE1α and XBP1s[137] significantly and further induce ER stress in kidneys. Interestingly, the *in vitro* experiment showed that inhibiting the ER stress IRE1α pathway can reverse the decrement of viability and insulin sensitivity in NBP-mediated renal tubular epithelial cells, which demonstrated that ER stress related IRE1α signaling can mediate the nephrotoxicity including ER stress and insensitivity induced by NBP. Fortunately, Raman spectra revealed that the concentration of $PO_4^{3-}$ in the urine of mice rose sharply within 12 hours after BPQD injection. $PO_4^{3-}$ is consistent with the product obtained by oxidation of BP in air, and this made them speculate that BPQDs in *in vivo* surroundings can be degraded to phosphate and excreted through urine.[28]

**4.2.4 Developmental toxicity of NBP.** A previous study[138] showed that 2D graphene oxide can affect the development of zebrafish embryo through chorion damage, oxidative stress, mitochondrial toxicity and so on. Similarly, Yang *et al.*[139] discovered that NBP with an average thickness of 60 nm and −23.6 mV zeta potential also affected the development of zebrafish embryo. Their NBP could aggregate on the chorion surface, then gradually penetrate into zebrafish embryo. By investigating the indicators of hatching, survival, morphology and heart rate during embryogenesis, NBP with a dosage of 50 mg $L^{-1}$ significantly decreased the hatching rate at 72 hours post fertilization and caused 100% death at 96 hours post fertilization. The development of malformations such as spinal curvature, pericardial edema and yolk sac edema occurred in embryos after 96 hours of treatment of 20 mg $L^{-1}$ NBP. The average heart rate of zebrafish of the NBP treated group decreased in a concentration-dependent manner compared with that of the control group (169 beats per minutes). Since heart development plays an important role in zebrafish embryogenesis,[140,141] the author quantified the blood flow in the caudal of zebrafish. It was found that no red blood cells (RBCs) can be examined in the heart area of zebrafish embryo (Fig. 13A), and 10 mg $L^{-1}$ of NBP caused abnormality in the cardiovascular system of zebrafish embryo and significantly slowed the blood circulation by 91.3% compared to the untreated group (Fig. 13B and C). Results of the transcriptomic analysis on embryos of zebrafish demonstrated that 2 mg $L^{-1}$ NBP treatment disrupted the

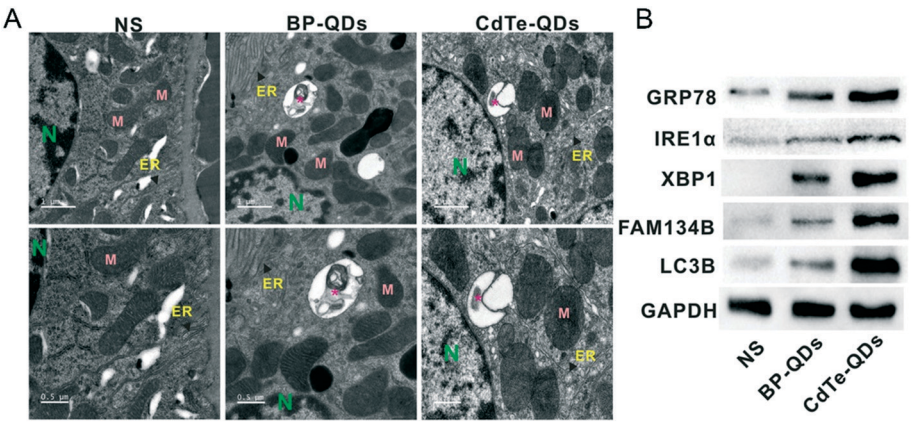


Fig. 12 ER stress in kidneys caused by NBP and CdTe quantum dots in mice. A) TEM image showing ER swelling (arrow) and ER-phagy (asterisks) in the tissue of kidneys. Scale bar of upper panels: 1 μm, scale bar of lower panels: 0.5 μm. B) Level of proteins including ER stress (GRP78, IRE1α, and XBP1) and ER-phagy (FAM134B and LC3B) examined by western blot.[133] Reprinted from He *et al.* Copyright the 2020 WILEY-VCH Verlag GmbH & Co. KGaA, Weinheim.

 

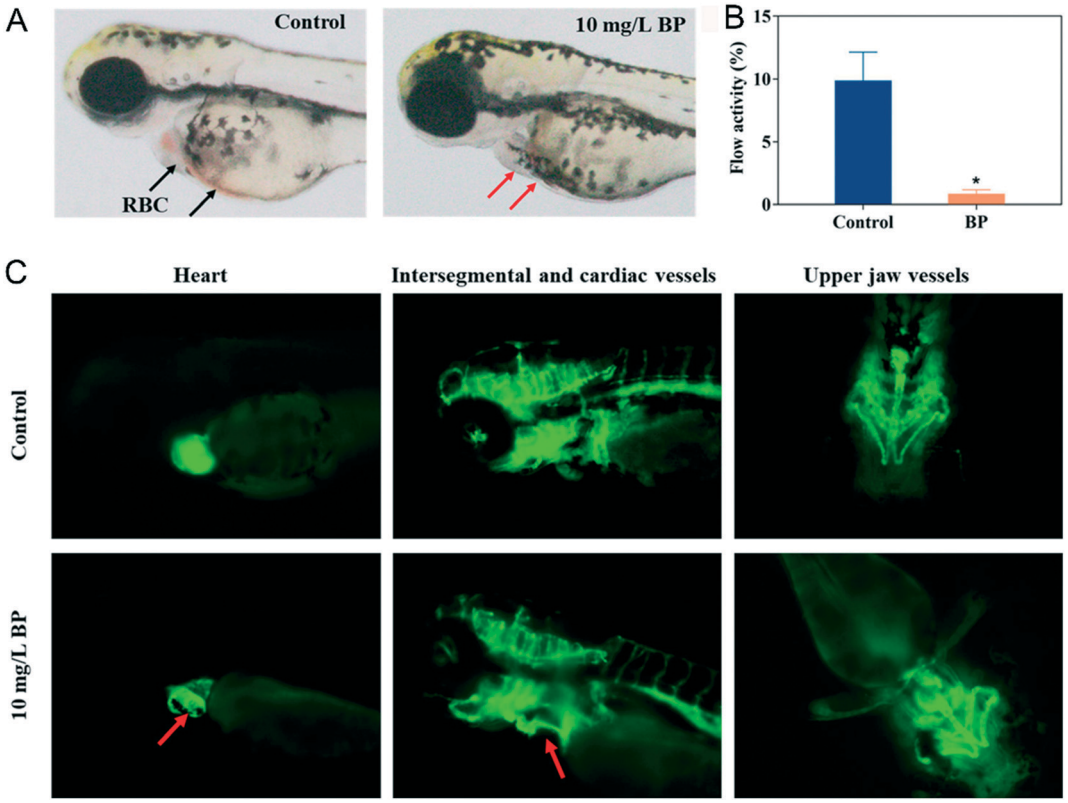


**Fig. 13** Effect of NBP on the cardiovascular system in zebrafish. A) Morphology of red blood cells (RBCs) in zebrafish of the control group and 10 mg $L^{-1}$ NBP treatment group at 96 hours post fertilization. The red arrows show the absence of RBCs after NBP treatment. B) Blood flow activity of zebrafish under 10 mg $L^{-1}$ NBP treatment at 96 hours post fertilization, $*p < 0.05$ compared with the control group. C) The red arrows denote the enlarged heart and abnormal cardiac vessels.[139] Reprinted from Yang *et al.* Copyright the © 2020 American Chemical Society.

signaling pathway related genes associated with muscle development, focal adhesion, oxygen involving process and so on.

## 5 Conclusion

As novel 2D nanomaterials with excellent fluorescence performance, high photothermal conversion, and large drug loading capacity, various NBPs have been designed and applied in biosensing, bioimaging, therapy and drug delivery. However, similar to other types of 2D nanomaterials, the toxicity concern and exposure risk hinder their wide biological applications. Here, we introduced different preparation and functionalization methods to improve the stability, biocompatibility, photothermal conversion efficiency or ROS generation of NBP for bioengineering applications. The important parameters of fabrication were analyzed in detail. Meanwhile, the biomedical applications of NBP, including biosensing, fluorescence/photoacoustics/photothermal imaging, photothermal/photodynamic therapy and drug delivery, were discussed. In addition, the toxicity assessment of NBP for cells and animals was emphasized from *in vitro* nano–bio interaction to toxic effects for various systems in animals.

Although the rapid development of NBP has shown excellent merits and great potential for bioengineering applications, there are still two huge challenges to be addressed before practical clinics. 1) The biodistribution and exposure risk of NBPs should be investigated extensively before they are applied in clinics. Besides the immune system, urinary system, and reproductive system, the interactions between the circulation/nervous/genetic/digestive/respiratory system and NBP should be studied systematically. 2) A standardized protocol should be set up to evaluate the toxicity of various NBPs. The reported dosage and the treatment of NBP for cells and animals from different research groups differed sharply, which makes it impossible to compare the toxicity of various NBPs. It also hinders the optimization and improvement of biocompatible NBP.

With this review, we hope to encourage further exploitation of NBPs to develop more practical nanomaterials for biomedical applications.

## Author contributions

Na Wu and Xiaomei Wang co-wrote the original manuscript. Chandreyee Manas Das reviewed and edited the paper. Mingze Ma conducted formal analysis. Nan Qiao completed the data curation. Taojian Fan wrote the manuscript about

chemistry. Han Zhang performed the project administration. Gaixia Xu provided the conceptual framework for this study. Ken-Tye Yong supervised this work.

## Conflicts of interest

There are no conflicts to declare.

## Acknowledgements

This work was supported by the National Natural Science Foundation of China (81772002&81801859), Natural Science Foundation of Guangdong Province (2021A1010012159&2019A1515012163), Guangdong Medical Science and Technology Research Funding (A2019359), Subject Layout Project of Shenzhen Science and Technology Creation Commission (JCYJ20170818092553608), Shenzhen Stability Support Program for Universities (20200812122708001) and Start-up Grant from Shenzhen University (2019136).

## References

1 K. S. Novoselov, A. K. Geim, S. V. Morozov, D. Jiang, Y. Zhang and S. V. Dubonos, *et al.*, Electric Field Effect in Atomically Thin Carbon Films, *Science*, 2004, **306**(5696), 666–669.
2 D. Unuchek, A. Ciarrocchi, A. Avsar, K. Watanabe, T. Taniguchi and A. Kis, Room-temperature electrical control of exciton flux in a van der Waals heterostructure, *Nature*, 2018, **560**(7718), 340–344.
3 Z. Lin, Y. Liu, U. Halim, M. Ding, Y. Liu and Y. Wang, *et al.*, Solution-processable 2D semiconductors for high-performance large-area electronics, *Nature*, 2018, **562**(7726), 254–258.
4 J. Ouyang, C. Feng, X. Ji, L. Li, H. K. Gutti and N. Y. Kim, *et al.*, 2D Monoelemental Germanene Quantum Dots: Synthesis as Robust Photothermal Agents for Photonic Cancer Nanomedicine, *Angew. Chem., Int. Ed.*, 2019, **58**(38), 13405–13410.
5 W. Tao, N. Kong, X. Ji, Y. Zhang, A. Sharma and J. Ouyang, *et al.*, Emerging two-dimensional monoelemental materials (Xenes) for biomedical applications, *Chem. Soc. Rev.*, 2019, **48**(11), 2891–2912.
6 W. Chen, C. Liu, X. Ji, J. Joseph, Z. Tang and J. Ouyang, *et al.*, Stanene-Based Nanosheets for beta-Elemene Delivery and Ultrasound-Mediated Combination Cancer Therapy, *Angew. Chem., Int. Ed.*, 2021, **60**(13), 7155–7164.
7 P. Gao, Y. Xiao, Y. Wang, L. Li, W. Li and W. Tao, Biomedical applications of 2D monoelemental materials formed by group VA and VIA: a concise review, *J. Nanobiotechnol.*, 2021, **19**(1), 96.
8 J. Ouyang, L. Zhang, L. Li, W. Chen, Z. Tang and X. Ji, *et al.*, Cryogenic Exfoliation of 2D Stanene Nanosheets for Cancer Theranostics, *Nano-Micro Lett.*, 2021, **13**(1), 90.
9 C. Feng, J. Ouyang, Z. Tang, N. Kong, Y. Liu and L. Fu, *et al.*, Germanene-Based Theranostic Materials for Surgical Adjuvant Treatment: Inhibiting Tumor Recurrence and Wound Infection, *Matter*, 2020, **3**(1), 127–144.
10 C. Liu, J. Shin, S. Son, Y. Choe, N. Farokhzad and Z. Tang, *et al.*, Pnictogens in medicinal chemistry: evolution from erstwhile drugs to emerging layered photonic nanomedicine, *Chem. Soc. Rev.*, 2021, **50**(4), 2260–2279.
11 L. Li, Y. Yu, G. J. Ye, Q. Ge, X. Ou and H. Wu, *et al.*, Black phosphorus field-effect transistors, *Nat. Nanotechnol.*, 2014, **9**(5), 372–377.
12 Q. Zhou, Q. Chen, Y. Tong and J. Wang, Light-Induced Ambient Degradation of Few-Layer Black Phosphorus: Mechanism and Protection, *Angew. Chem., Int. Ed.*, 2016, **55**(38), 11437–11441.
13 T. Y. Chang, P. L. Chen, J. H. Yan, W. Q. Li, Y. Y. Zhang and D. I. Luo, *et al.*, Ultra-Broadband, High Speed, and High-Quantum-Efficiency Photodetectors Based on Black Phosphorus, *ACS Appl. Mater. Interfaces*, 2020, **12**(1), 1201–1209.
14 J. Zhou, Z. Li, M. Ying, M. Liu, X. Wang and X. Wang, *et al.*, Black phosphorus nanosheets for rapid microRNA detection, *Nanoscale*, 2018, **10**(11), 5060–5064.
15 P. Chellan and P. J. Sadler, The elements of life and medicines, *Philos. Trans. R. Soc., A*, 2015, **373**, 20140182.
16 H. Wang and X. F. Yu, Few-Layered Black Phosphorus: From Fabrication and Customization to Biomedical Applications, *Small*, 2018, **14**(6), 1702830.
17 M. Fojtů, X. Chia, Z. Sofer, M. Masařík and M. Pumera, Black Phosphorus Nanoparticles Potentiate the Anticancer Effect of Oxaliplatin in Ovarian Cancer Cell Line, *Adv. Funct. Mater.*, 2017, **27**(36), 1701955.
18 Z. Tang, N. Kong, J. Ouyang, C. Feng, N. Y. Kim and X. Ji, *et al.*, Phosphorus Science-Oriented Design and Synthesis of Multifunctional Nanomaterials for Biomedical Applications, *Matter*, 2020, **2**(2), 297–322.
19 W. Ou, J. H. Byeon, R. K. Thapa, S. K. Ku, C. S. Yong and J. O. Kim, Plug-and-Play Nanorization of Coarse Black Phosphorus for Targeted Chemo-photoimmunotherapy of Colorectal Cancer, *ACS Nano*, 2018, **12**(10), 10061–10074.
20 J. R. Choi, K. W. Yong, J. Y. Choi, A. Nilghaz, Y. Lin and J. Xu, *et al.*, Black Phosphorus and its Biomedical Applications, *Theranostics*, 2018, **8**(4), 1005–1026.
21 M. Qiu, W. X. Ren, T. Jeong, M. Won, G. Y. Park and D. K. Sang, *et al.*, Omnipotent phosphorene: a next-generation, two-dimensional nanoplatform for multidisciplinary biomedical applications, *Chem. Soc. Rev.*, 2018, **47**(15), 5588–5601.
22 K. T. Yong, W. C. Law, R. Hu, L. Ye, L. Liu and M. T. Swihart, *et al.*, Nanotoxicity assessment of quantum dots: from cellular to primate studies, *Chem. Soc. Rev.*, 2013, **42**(3), 1236–1250.
23 G. X. Xu, S. W. Zeng, B. T. Zhang, M. T. Swihart, K. T. Yong and P. N. Prasad, New Generation Cadmium-Free Quantum Dots for Biophotonics and Nanomedicine, *Chem. Rev.*, 2016, **116**(19), 12234–12327.
24 K. Yang, Y. Li, X. Tan, R. Peng and Z. Liu, Behavior and toxicity of graphene and its functionalized derivatives in biological systems, *Small*, 2013, **9**(9–10), 1492–1503.

 

25 J. I. Paredes, J. M. Munuera, S. Villar-Rodil, L. Guardia, M. Ayan-Varela and A. Pagan, *et al.*, Impact of Covalent Functionalization on the Aqueous Processability, Catalytic Activity, and Biocompatibility of Chemically Exfoliated $MoS_2$ Nanosheets, *ACS Appl. Mater. Interfaces*, 2016, **8**(41), 27974–27986.

26 H. U. Lee, S. Y. Park, S. C. Lee, S. Choi, S. Seo and H. Kim, *et al.*, Black Phosphorus (BP) Nanodots for Potential Biomedical Applications, *Small*, 2016, **12**(2), 214–219.

27 N. Gao, J. Nie, H. Wang, C. Xing, L. Mei and W. Xiong, *et al.*, A Versatile Platform Based on Black Phosphorus Nanosheets with Enhanced Stability for Cancer Synergistic Therapy, *J. Biomed. Nanotechnol.*, 2018, **14**(11), 1883–1897.

28 X. Mu, J. Y. Wang, X. Bai, F. Xu, H. Liu and J. Yang, *et al.*, Black Phosphorus Quantum Dot Induced Oxidative Stress and Toxicity in Living Cells and Mice, *ACS Appl. Mater. Interfaces*, 2017, **9**(24), 20399–20409.

29 G. Abellan, S. Wild, V. Lloret, N. Scheuschner, R. Gillen and U. Mundloch, *et al.*, Fundamental Insights into the Degradation and Stabilization of Thin Layer Black Phosphorus, *J. Am. Chem. Soc.*, 2017, **139**(30), 10432–10440.

30 J. R. Brent, N. Savjani, E. A. Lewis, S. J. Haigh, D. J. Lewis and P. O'Brien, Production of few-layer phosphorene by liquid exfoliation of black phosphorus, *Chem. Commun.*, 2014, **50**(87), 13338–13341.

31 S. Lin, S. Liu, Z. Yang, Y. Li, T. W. Ng and Z. Xu, *et al.*, Solution-Processable Ultrathin Black Phosphorus as an Effective Electron Transport Layer in Organic Photovoltaics, *Adv. Funct. Mater.*, 2016, **26**(6), 864–871.

32 Z. Guo, H. Zhang, S. Lu, Z. Wang, S. Tang and J. Shao, *et al.*, From Black Phosphorus to Phosphorene: Basic Solvent Exfoliation, Evolution of Raman Scattering, and Applications to Ultrafast Photonics, *Adv. Funct. Mater.*, 2015, **25**(45), 6996–7002.

33 Z. Sun, H. Xie, S. Tang, X. F. Yu, Z. Guo and J. Shao, *et al.*, Ultrasmall Black Phosphorus Quantum Dots: Synthesis and Use as Photothermal Agents, *Angew. Chem., Int. Ed.*, 2015, **54**(39), 11526–11530.

34 H. Liu, A. T. Neal, Z. Zhu, Z. Luo, X. Xu, D. Tománek and P. D. Ye, Phosphorene: An Unexplored 2D Semiconductor with a High Hole Mobility, *ACS Nano*, 2014, **8**(4), 4033–4041.

35 Z. Sofer, D. Bousa, J. Luxa, V. Mazanek and M. Pumera, Few-layer black phosphorus nanoparticles, *Chem. Commun.*, 2016, **52**(8), 1563–1566.

36 Z. Yan, X. He, L. She, J. Sun, R. Jiang and H. Xu, *et al.*, Solvothermal-assisted liquid-phase exfoliation of large size and high quality black phosphorus, *Journal of Materiomics*, 2018, **4**(2), 129–134.

37 Y. Xu, Z. Wang, Z. Guo, H. Huang, Q. Xiao and H. Zhang, *et al.*, Solvothermal Synthesis and Ultrafast Photonics of Black Phosphorus Quantum Dots, *Adv. Opt. Mater.*, 2016, **4**(8), 1223–1229.

38 W. Chen, J. Ouyang, X. Yi, Y. Xu, C. Niu and W. Zhang, *et al.*, Black Phosphorus Nanosheets as a Neuroprotective Nanomedicine for Neurodegenerative Disorder Therapy, *Adv. Mater.*, 2018, **30**(3), 1703458.

39 C. C. Mayorga-Martinez, N. Mohamad Latiff, A. Y. S. Eng, Z. Sofer and M. Pumera, Black Phosphorus Nanoparticle Labels for Immunoassays via Hydrogen Evolution Reaction Mediation, *Anal. Chem.*, 2016, **88**(20), 10074–10079.

40 X. Ren, F. Zhang and X. Zhang, Synthesis of Black Phosphorus Quantum Dots with High Quantum Yield by Pulsed Laser Ablation for Cell Bioimaging, *Chem. – Asian J.*, 2018, **13**(14), 1842–1846.

41 S. Ge, L. Zhang, P. Wang and Y. Fang, Intense, stable and excitation wavelength-independent photoluminescence emission in the blue-violet region from phosphorene quantum dots, *Sci. Rep.*, 2016, **6**, 27307.

42 Y. Huang, J. Qiao, K. He, S. Bliznakov, E. Sutter and X. Chen, *et al.*, Interaction of Black Phosphorus with Oxygen and Water, *Chem. Mater.*, 2016, **28**(22), 8330–8339.

43 A. Favron, E. Gaufres, F. Fossard, A. L. Phaneuf-L'Heureux, N. Y. Tang and P. L. Levesque, *et al.*, Photooxidation and quantum confinement effects in exfoliated black phosphorus, *Nat. Mater.*, 2015, **14**(8), 826–832.

44 W. Liu, Y. Zhang, Y. Zhang and A. Dong, Black Phosphorus Nanosheets Counteract Bacteria without Causing Antibiotic Resistance, *Chem. - Eur. J.*, 2020, **26**(11), 2478–2485.

45 J. Mo, Q. Xie, W. Wei and J. Zhao, Revealing the immune perturbation of black phosphorus nanomaterials to macrophages by understanding the protein corona, *Nat. Commun.*, 2018, **9**(1), 2480.

46 B. K. Poudel, J. Hwang, S. K. Ku, J. O. Kim and J. H. Byeon, A batch-by-batch free route for the continuous production of black phosphorus nanosheets for targeted combination cancer therapy, *NPG Asia Mater.*, 2018, **10**(8), 727–739.

47 Y. Li, Z. Liu, Y. Hou, G. Yang, X. Fei and H. Zhao, *et al.*, Multifunctional Nanoplatform Based on Black Phosphorus Quantum Dots for Bioimaging and Photodynamic/Photothermal Synergistic Cancer Therapy, *ACS Appl. Mater. Interfaces*, 2017, **9**(30), 25098–25106.

48 J. Shao, H. Xie, H. Huang, Z. Li, Z. Sun and Y. Xu, *et al.*, Biodegradable black phosphorus-based nanospheres for in vivo photothermal cancer therapy, *Nat. Commun.*, 2016, **7**, 12967.

49 S. Geng, L. Wu, H. Cui, W. Tan, T. Chen and P. K. Chu, *et al.*, Synthesis of lipid-black phosphorus quantum dot bilayer vesicles for near-infrared-controlled drug release, *Chem. Commun.*, 2018, **54**(47), 6060–6063.

50 S. Wang, J. Weng, X. Fu, J. Lin, W. Fan and N. Lu, *et al.*, Black Phosphorus Nanosheets for Mild Hyperthermia-Enhanced Chemotherapy and Chemo-Photothermal Combination Therapy, *Nanotheranostics*, 2017, **1**(2), 208–216.

51 J. Ouyang, X. Ji, X. Zhang, C. Feng, Z. Tang and N. Kong, *et al.*, In situ sprayed NIR-responsive, analgesic black phosphorus-based gel for diabetic ulcer treatment, *Proc. Natl. Acad. Sci. U. S. A.*, 2020, **117**(46), 28667–28677.

52 S. Walia, S. Balendhran, T. Ahmed, M. Singh, C. El-Badawi and M. D. Brennan, *et al.*, Ambient Protection of Few-Layer Black Phosphorus via Sequestration of Reactive Oxygen Species, *Adv. Mater.*, 2017, **29**(27), 1700152.

53 X. Yang, D. Wang, Y. Shi, J. Zou, Q. Zhao and Q. Zhang, *et al.*, Black Phosphorus Nanosheets Immobilizing Ce6 for Imaging-Guided Photothermal/Photodynamic Cancer Therapy, *ACS Appl. Mater. Interfaces*, 2018, **10**(15), 12431–12440.

54 G. Yang, Z. Liu, Y. Li, Y. Hou, X. Fei and C. Su, *et al.*, Facile synthesis of black phosphorus-Au nanocomposites for enhanced photothermal cancer therapy and surface-enhanced Raman scattering analysis, *Biomater. Sci.*, 2017, **5**(10), 2048–2055.

55 J. Shao, C. Ruan, H. Xie, Z. Li, H. Wang and P. K. Chu, *et al.*, Black-Phosphorus-Incorporated Hydrogel as a Sprayable and Biodegradable Photothermal Platform for Postsurgical Treatment of Cancer, *Adv. Sci.*, 2018, **5**(5), 1700848.

56 H. Wang, X. Yang, W. Shao, S. Chen, J. Xie and X. Zhang, *et al.*, Ultrathin Black Phosphorus Nanosheets for Efficient Singlet Oxygen Generation, *J. Am. Chem. Soc.*, 2015, **137**(35), 11376–11382.

57 H. Huang, L. He, W. Zhou, G. Qu, J. Wang and N. Yang, *et al.*, Stable black phosphorus/$Bi_2O_3$ heterostructures for synergistic cancer radiotherapy, *Biomaterials*, 2018, **171**, 12–22.

58 D. Zhang, X. Lin, S. Lan, H. Sun, X. Wang and X. Liu, *et al.*, Localized Surface Plasmon Resonance Enhanced Singlet Oxygen Generation and Light Absorption Based on Black Phosphorus@AuNPs Nanosheet for Tumor Photodynamic/Thermal Therapy, *Part. Part. Syst. Charact.*, 2018, **35**(4), 1800010.

59 J. Liu, P. Du, H. Mao, L. Zhang, H. Ju and J. Lei, Dual-triggered oxygen self-supply black phosphorus nanosystem for enhanced photodynamic therapy, *Biomaterials*, 2018, **172**, 83–91.

60 F. Xia, H. Wang, D. Xiao, M. Dubey and A. Ramasubramaniam, Two-dimensional material nanophotonics, *Nat. Photonics*, 2014, **8**(12), 899–907.

61 X. Ge, Z. Xia and S. Guo, Recent Advances on Black Phosphorus for Biomedicine and Biosensing, *Adv. Funct. Mater.*, 2019, **29**(29), 1900318.

62 J. Peng, Y. Lai, Y. Chen, J. Xu, L. Sun and J. Weng, Sensitive Detection of Carcinoembryonic Antigen Using Stability-Limited Few-Layer Black Phosphorus as an Electron Donor and a Reservoir, *Small*, 2017, **13**(15), 1603589.

63 S. K. Tuteja and S. Neethirajan, Exploration of two-dimensional bio-functionalized phosphorene nanosheets (black phosphorous) for label free haptoglobin electro-immunosensing applications, *Nanotechnology*, 2018, **29**(13), 135101.

64 H. Liu, H. Yin, Y. Dong, H. Ding and X. ChuElectrochemiluminescence resonance energy transfer between luminol and black phosphorus nanosheets for the detection of trypsin via the "off-on-off" switch mode, *Analyst*, 2020, **145**(6), 2204–2211.

65 L. Zhou, C. Liu, Z. Sun, H. Mao, L. Zhang and X. Yu, *et al.*, Black phosphorus based fiber optic biosensor for ultrasensitive cancer diagnosis, *Biosens. Bioelectron.*, 2019, **137**, 140–147.

66 A. Castellanos-Gomez, L. Vicarelli, E. Prada, J. O. Island, K. L. Narasimha-Acharya and S. I. Blanter, *et al.*, Isolation and characterization of few-layer black phosphorus, *2D Mater.*, 2014, **1**(2), 025001.

67 Y. C. Shin, S. J. Song, Y. B. Lee, M. S. Kang, H. U. Lee and J. W. Oh, *et al.*, Application of black phosphorus nanodots to live cell imaging, *Biomater. Res.*, 2018, **22**, 31.

68 S. Kunjachan, J. Ehling, G. Storm, F. Kiessling and T. Lammers, Noninvasive Imaging of Nanomedicines and Nanotheranostics: Principles, Progress, and Prospects, *Chem. Rev.*, 2015, **115**(19), 10907–10937.

69 L. Deng, Y. Xu, C. Sun, B. Yun, Q. Sun and C. Zhao, *et al.*, Functionalization of small black phosphorus nanoparticles for targeted imaging and photothermal therapy of cancer, *Sci. Bull.*, 2018, **63**(14), 917–924.

70 Z. Sun, Y. Zhao, Z. Li, H. Cui, Y. Zhou and W. Li, *et al.*, TiL4 -Coordinated Black Phosphorus Quantum Dots as an Efficient Contrast Agent for In Vivo Photoacoustic Imaging of Cancer, *Small*, 2017, **13**(11), 1602896.

71 Z. Sun, Y. Zhang, H. Yu, C. Yan, Y. Liu and S. Hong, *et al.*, New solvent-stabilized few-layer black phosphorus for antibacterial applications, *Nanoscale*, 2018, **10**(26), 12543–12553.

72 A. Naskar and K. S. Kim, Black phosphorus nanomaterials as multi-potent and emerging platforms against bacterial infections, *Microb. Pathog.*, 2019, **137**, 103800.

73 J. Ouyang, C. Feng, X. Zhang, N. Kong and W. Tao, Black Phosphorus in Biological Applications: Evolutionary Journey from Monoelemental Materials to Composite Materials, *Acc. Mater. Res.*, 2021, **2**(7), 489–500.

74 Y. Zhao, H. Wang, H. Huang, Q. Xiao, Y. Xu and Z. Guo, *et al.*, Surface Coordination of Black Phosphorus for Robust Air and Water Stability, *Angew. Chem., Int. Ed.*, 2016, **55**(16), 5003–5007.

75 B. Le Ouay and F. Stellacci, Antibacterial activity of silver nanoparticles: A surface science insight, *Nano Today*, 2015, **10**(3), 339–354.

76 J. Ouyang, R.-Y. Liu, W. Chen, Z. Liu, Q. Xu and K. Zeng, *et al.*, A black phosphorus based synergistic antibacterial platform against drug resistant bacteria, *J. Mater. Chem. B*, 2018, **6**(39), 6302–6310.

77 X. W. Huang, J. J. Wei, M. Y. Zhang, X. L. Zhang, X. F. Yin and C. H. Lu, *et al.*, Water-Based Black Phosphorus Hybrid Nanosheets as a Moldable Platform for Wound Healing Applications, *ACS Appl. Mater. Interfaces*, 2018, **10**(41), 35495–35502.

78 C. Mao, Y. Xiang, X. Liu, Z. Cui, X. Yang and Z. Li, *et al.*, Repeatable Photodynamic Therapy with Triggered Signaling Pathways of Fibroblast Cell Proliferation and Differentiation To Promote Bacteria-Accompanied Wound Healing, *ACS Nano*, 2018, **12**(2), 1747–1759.

 

79 K. Hu, L. Xie, Y. Zhang, M. Hanyu, Z. Yang and K. Nagatsu, *et al.*, Marriage of black phosphorus and Cu(2+) as effective photothermal agents for PET-guided combination cancer therapy, *Nat. Commun.*, 2020, **11**(1), 2778.

80 M. Wang, Y. Liang, Y. Liu, G. Ren, Z. Zhang and S. Wu, *et al.*, Ultrasmall black phosphorus quantum dots: synthesis, characterization, and application in cancer treatment, *Analyst*, 2018, **143**(23), 5822–5833.

81 C. Sun, L. Wen, J. Zeng, Y. Wang, Q. Sun and L. Deng, *et al.*, One-pot solventless preparation of PEGylated black phosphorus nanoparticles for photoacoustic imaging and photothermal therapy of cancer, *Biomaterials*, 2016, **91**, 81–89.

82 C. Xing, S. Chen, M. Qiu, X. Liang, Q. Liu and Q. Zou, *et al.*, Conceptually Novel Black Phosphorus/Cellulose Hydrogels as Promising Photothermal Agents for Effective Cancer Therapy, *Adv. Healthcare Mater.*, 2018, **7**(7), e1701510.

83 X. Wang, J. Shao, M. Abd El Raouf, H. Xie, H. Huang and H. Wang, *et al.*, Near-infrared light-triggered drug delivery system based on black phosphorus for in vivo bone regeneration, *Biomaterials*, 2018, **179**, 164–174.

84 L. Tong, Q. Liao, Y. Zhao, H. Huang, A. Gao and W. Zhang, *et al.*, Near-infrared light control of bone regeneration with biodegradable photothermal osteoimplant, *Biomaterials*, 2019, **193**, 1–11.

85 Z. Li, X. Zhang, J. Ouyang, D. Chu, F. Han and L. Shi, *et al.*, Ca(2+)-supplying black phosphorus-based scaffolds fabricated with microfluidic technology for osteogenesis, *Bioact. Mater.*, 2021, **6**(11), 4053–4064.

86 H. Xie, J. Shao, Y. Ma, J. Wang, H. Huang and N. Yang, *et al.*, Biodegradable near-infrared-photoresponsive shape memory implants based on black phosphorus nanofillers, *Biomaterials*, 2018, **164**, 11–21.

87 N. Kong, X. Ji, J. Wang, X. Sun, G. Chen and T. Fan, *et al.*, ROS-Mediated Selective Killing Effect of Black Phosphorus: Mechanistic Understanding and Its Guidance for Safe Biomedical Applications, *Nano Lett.*, 2020, **20**(5), 3943–3955.

88 T. Guo, Y. Wu, Y. Lin, X. Xu, H. Lian and G. Huang, *et al.*, Black Phosphorus Quantum Dots with Renal Clearance Property for Efficient Photodynamic Therapy, *Small*, 2018, **14**(4), 1702815.

89 J. Liu, P. Du, T. Liu, B. J. Cordova Wong, W. Wang and H. Ju, *et al.*, A black phosphorus/manganese dioxide nanoplatform: Oxygen self-supply monitoring, photodynamic therapy enhancement and feedback, *Biomaterials*, 2019, **192**, 179–188.

90 D. Yang, G. Yang, P. Yang, R. Lv, S. Gai and C. Li, *et al.*, Assembly of Au Plasmonic Photothermal Agent and Iron Oxide Nanoparticles on Ultrathin Black Phosphorus for Targeted Photothermal and Photodynamic Cancer Therapy, *Adv. Funct. Mater.*, 2017, **27**(18), 1700371.

91 Z. Li, Y. Hu, Q. Fu, Y. Liu, J. Wang and J. Song, *et al.*, NIR/ROS-Responsive Black Phosphorus QD Vesicles as Immunoadjuvant Carrier for Specific Cancer Photodynamic Immunotherapy, *Adv. Funct. Mater.*, 2020, **30**(3), 1905758.

92 Q. Yin, J. Shen, Z. Zhang, H. Yu and Y. Li, Reversal of multidrug resistance by stimuli-responsive drug delivery systems for therapy of tumor, *Adv. Drug Delivery Rev.*, 2013, **65**(13–14), 1699–1715.

93 G. Yang, X. Wan, Z. Gu, X. Zeng and J. Tang, Near infrared photothermal-responsive poly(vinyl alcohol)/black phosphorus composite hydrogels with excellent on-demand drug release capacity, *J. Mater. Chem. B*, 2018, **6**(11), 1622–1632.

94 W. Tao, X. Zhu, X. Yu, X. Zeng, Q. Xiao and X. Zhang, *et al.*, Black Phosphorus Nanosheets as a Robust Delivery Platform for Cancer Theranostics, *Adv. Mater.*, 2017, **29**(1), 1603276.

95 F. Yin, K. Hu, S. Chen, D. Wang, J. Zhang and M. Xie, *et al.*, Black phosphorus quantum dot based novel siRNA delivery systems in human pluripotent teratoma PA-1 cells, *J. Mater. Chem. B*, 2017, **5**(27), 5433–5440.

96 W. Zhou, H. Cui, L. Ying and X. F. Yu, Enhanced Cytosolic Delivery and Release of CRISPR/Cas9 by Black Phosphorus Nanosheets for Genome Editing, *Angew. Chem., Int. Ed.*, 2018, **57**(32), 10268–10272.

97 L. Jin, P. Hu, Y. Wang, L. Wu, K. Qin and H. Cheng, *et al.*, Fast-Acting Black-Phosphorus-Assisted Depression Therapy with Low Toxicity, *Adv. Mater.*, 2020, **32**(2), e1906050.

98 Z. Tang, Y. Xiao, N. Kong, C. Liu, W. Chen and X. Huang, *et al.*, Nano-bio interfaces effect of two-dimensional nanomaterials and their applications in cancer immunotherapy, *Acta Pharm. Sin. B*, 2021, **05**(004), DOI: 10.1016/j.apsb.2021.05.004.

99 J. O. Island, G. A. Steele, H. S. J. Zant and A. Castellanos-Gomez, Environmental instability of few-layer black phosphorus, *2D Mater.*, 2015, **2**, 011002.

100 L. M. Guiney, X. Wang, T. Xia, A. E. Nel and M. C. Hersam, Assessing and Mitigating the Hazard Potential of Two-Dimensional Materials, *ACS Nano*, 2018, **12**(7), 6360–6377.

101 M. Fojtů, W. Z. Teo and M. Pumera, Environmental impact and potential health risks of 2D nanomaterials, *Environ. Sci.: Nano*, 2017, **4**(8), 1617–1633.

102 S. J. Song, Y. C. Shin, H. U. Lee, B. Kim, D. W. Han and D. Lim, Dose- and Time-Dependent Cytotoxicity of Layered Black Phosphorus in Fibroblastic Cells, *Nanomaterials*, 2018, **8**, 408.

103 Y. Schneider, P. Chabert, J. Stutzmann, D. Coelho, A. Fougerousse and F. Gosse, *et al.*, Resveratrol analog (Z)-3,5,4′-trimethoxystilbene is a potent anti-mitotic drug inhibiting tubulin polymerization, *Int. J. Cancer*, 2003, **107**(2), 189–196.

104 Z. Xiong, X. Zhang, S. Zhang, L. Lei, W. Ma and D. Li, *et al.*, Bacterial toxicity of exfoliated black phosphorus nanosheets, *Ecotoxicol. Environ. Saf.*, 2018, **161**, 507–514.

105 X. Zhang, Z. Zhang, S. Zhang, D. Li, W. Ma and C. Ma, *et al.*, Size Effect on the Cytotoxicity of Layered Black Phosphorus and Underlying Mechanisms, *Small*, 2017, **13**(32), 1701210.

106 Y. Tu, M. Lv, P. Xiu, T. Huynh, M. Zhang and M. Castelli, *et al.*, Destructive extraction of phospholipids from Escherichia coli membranes by graphene nanosheets, *Nat. Nanotechnol.*, 2013, **8**(8), 594–601.

107 O. Akhavan and E. Ghaderi, Toxicity of Graphene and Graphene Oxide Nanowalls Against Bacteria, *ACS Nano*, 2010, **4**(10), 5731–5736.
108 T. Guo, S. Zhuang, H. Qiu, Y. Guo, L. Wang and G. Jin, *et al.*, Black Phosphorus Nanosheets for Killing Bacteria through Nanoknife Effect, *Part. Part. Syst. Charact.*, 2020, **37**(8), 2000169.
109 Q. Wu, L. Yao, X. Zhao, L. Zeng, P. Li and X. Yang, *et al.*, Cellular Uptake of Few-Layered Black Phosphorus and the Toxicity to an Aquatic Unicellular Organism, *Environ. Sci. Technol.*, 2020, **54**(3), 1583–1592.
110 Y. Sun, S. Fan, S. Fan, C. Li, Z. Shang and M. Gu, *et al.*, In Vitro and In Vivo Toxicity of Black Phosphorus Nanosheets, *J. Nanosci. Nanotechnol.*, 2020, **20**(2), 659–667.
111 M. Valko, D. Leibfritz, J. Moncol, M. T. Cronin, M. Mazur and J. Telser, Free radicals and antioxidants in normal physiological functions and human disease, *Int. J. Biochem. Cell Biol.*, 2007, **39**(1), 44–84.
112 G. Qu, W. Liu, Y. Zhao, J. Gao, T. Xia and J. Shi, *et al.*, Improved Biocompatibility of Black Phosphorus Nanosheets by Chemical Modification, *Angew. Chem., Int. Ed.*, 2017, **56**(46), 14488–14493.
113 D. Wu, Y. Ma, Y. Cao and T. Zhang, Mitochondrial toxicity of nanomaterials, *Sci. Total Environ.*, 2020, **702**, 134994.
114 X. Zhu, X. Ji, N. Kong, Y. Chen, M. Mahmoudi and X. Xu, *et al.*, Intracellular Mechanistic Understanding of 2D $MoS_2$ Nanosheets for Anti-Exocytosis-Enhanced Synergistic Cancer Therapy, *ACS Nano*, 2018, **12**(3), 2922–2938.
115 K. S. Negara, K. Suwiyoga, T. G. A. Pemayun, A. A. R. Sudewi, N. M. Astawa and I. Arijana, *et al.*, The Role of Caspase-3, Apoptosis-Inducing Factor, and B-cell Lymphoma-2 Expressions in Term Premature Rupture of Membrane, *Rev. Bras. Ginecol. Obstet.*, 2018, **40**(12), 733–739.
116 Y. Wu, J. Zhuang, D. Zhao and C. Xu, Interaction between caspase-3 and caspase-5 in the stretch-induced programmed cell death in the human periodontal ligament cells, *J. Cell. Physiol.*, 2019, **234**(8), 13571–13581.
117 C. Moore, D. Movia, R. J. Smith, D. Hanlon, F. Lebre and E. C. Lavelle, *et al.*, Industrial grade 2D molybdenum disulphide ($MoS_2$): an in vitro exploration of the impact on cellular uptake, cytotoxicity, and inflammation, *2D Mater.*, 2017, **4**(2), 025065.
118 W. B. Hu, C. Peng, M. Lv, X. M. Li, Y. J. Zhang and N. Chen, *et al.*, Protein Corona-Mediated Mitigation of Cytotoxicity of Graphene Oxide, *ACS Nano*, 2011, **5**(5), 3693–3700.
119 N. M. Latiff, W. Z. Teo, Z. Sofer, A. C. Fisher and M. Pumera, The Cytotoxicity of Layered Black Phosphorus, *Chemistry*, 2015, **21**(40), 13991–13995.
120 M. Lee, Y. H. Park, E. B. Kang, A. Chae, Y. Choi and S. Jo, *et al.*, Highly Efficient Visible Blue-Emitting Black Phosphorus Quantum Dot: Mussel-Inspired Surface Functionalization for Bioapplications, *ACS Omega*, 2017, **2**(10), 7096–7105.
121 Y. Liu, J. Wang, Q. Xiong, D. Hornburg, W. Tao and O. C. Farokhzad, Nano-Bio Interactions in Cancer: From Therapeutics Delivery to Early Detection, *Acc. Chem. Res.*, 2021, **54**(2), 291–301.
122 H. Fu, Z. Li, H. Xie, Z. Sun, B. Wang and H. Huang, *et al.*, Different-sized black phosphorus nanosheets with good cytocompatibility and high photothermal performance, *RSC Adv.*, 2017, **7**(24), 14618–14624.
123 M. K. Song, S. D. Namgung, T. Sung, A. J. Cho, J. Lee and M. Ju, *et al.*, Physically Transient Field-Effect Transistors Based on Black Phosphorus, *ACS Appl. Mater. Interfaces*, 2018, **10**(49), 42630–42636.
124 S. J. Song, I. S. Raja, Y. B. Lee, M. S. Kang, H. J. Seo and H. U. Lee, *et al.*, Comparison of cytotoxicity of black phosphorus nanosheets in different types of fibroblasts, *Biomater. Res.*, 2019, **23**, 23.
125 G. Xu, G. Lin, S. Lin, N. Wu, Y. Deng and G. Feng, *et al.*, The Reproductive Toxicity of CdSe/ZnS Quantum Dots on the in vivo Ovarian Function and in vitro Fertilization, *Sci. Rep.*, 2016, **6**, 37677.
126 N. Wu, Z. Zhang, J. Zhou, Z. Sun, Y. Deng and G. Lin, *et al.*, The biocompatibility studies of polymer dots on pregnant mice and fetuses, *Nanotheranostics*, 2017, **1**(3), 261–271.
127 G. Qu, T. Xia, W. Zhou, X. Zhang, H. Zhang and L. Hu, *et al.*, Property–Activity Relationship of Black Phosphorus at the Nano– Bio Interface: From Molecules to Organisms, *Chem. Rev.*, 2020, **120**, 2288–2346.
128 S. Behzadi, V. Serpooshan, W. Tao, M. A. Hamaly, M. Y. Alkawareek and E. C. Dreaden, *et al.*, Cellular uptake of nanoparticles: journey inside the cell, *Chem. Soc. Rev.*, 2017, **46**(14), 4218–4244.
129 M. Hadjidemetriou and K. Kostarelos, Nanomedicine Evolution of the Nanoparticle Corona, *Nat. Nanotechnol.*, 2017, **12**(4), 288–290.
130 J. Chen, L. Lu, C. Zhang, X. Zhu and S. Zhuang, Endothelial dysfunction and transcriptome aberration in mouse aortas induced by black phosphorus quantum dots and nanosheets, *Nanoscale*, 2021, **13**(19), 9018–9030.
131 J. Mo, Y. Xu, X. Wang, W. Wei and J. Zhao, Exploiting the protein corona: coating of black phosphorus nanosheets enables macrophage polarization via calcium influx, *Nanoscale*, 2020, **12**(3), 1742–1748.
132 T. Liu, L. Zhang, D. Joo and S. C. Sun, NF-kappaB signaling in inflammation, *Signal Transduction Targeted Ther.*, 2017, **2**, 17023.
133 C. He, F. Ruan, S. Jiang, J. Zeng, H. Yin and R. Liu, *et al.*, Black Phosphorus Quantum Dots Cause Nephrotoxicity in Organoids, Mice, and Human Cells, *Small*, 2020, **16**(22), e2001371.
134 S. A. Patel, K. L. Hoehn, R. T. Lawrence, L. Sawbridge, N. A. Talbot and J. L. Tomsig, *et al.*, Overexpression of the adiponectin receptor AdipoR1 in rat skeletal muscle amplifies local insulin sensitivity, *Endocrinology*, 2012, **153**(11), 5231–5246.
135 S. Mao, L. Fang, F. Liu, S. Q. Jiang, L. X. Wu and J. H. Zhang, Leptin and chronic kidney diseases, *J. Recept. Signal Transduction*, 2018, **38**(2), 84–89.

 

136 C. Bravo, L. R. Cataldo, J. Galgani, J. Parada and J. L. Santos, Leptin/Adiponectin Ratios Using Either Total Or High-Molecular-Weight Adiponectin as Biomarkers of Systemic Insulin Sensitivity in Normoglycemic Women, *J. Diabetes Res.*, 2017, **2017**, 9031079.

137 R. Bravo, V. Parra, D. Gatica, A. E. Rodriguez, N. Torrealba and F. Paredes, *et al.*, Endoplasmic reticulum and the unfolded protein response: dynamics and metabolic integration, *Int. Rev. Cell Mol. Biol.*, 2013, **301**, 215–290.

138 A. Rhazouani, H. Gamrani, M. El Achaby, K. Aziz, L. Gebrati and M. S. Uddin, *et al.*, Synthesis and Toxicity of Graphene Oxide Nanoparticles: A Literature Review of In Vitro and In Vivo Studies, *BioMed Res. Int.*, 2021, **2021**, 5518999.

139 X. Yang, J. Liang, Q. Wu, M. Li, W. Shan and L. Zeng, *et al.*, Developmental Toxicity of Few-Layered Black Phosphorus toward Zebrafish, *Environ. Sci. Technol.*, 2021, **55**(2), 1134–1144.

140 J. Liu and D. Y. Stainier, Zebrafish in the study of early cardiac development, *Circ. Res.*, 2012, **110**(6), 870–874.

141 C. W. McCollum, N. A. Ducharme, M. Bondesson and J. A. Gustafsson, Developmental toxicity screening in zebrafish, *Birth Defects Res., Part C*, 2011, **93**(2), 67–114.